Robotica: (2020) volume 38, pp. 299–316. © Cambridge University Press 2019
doi:10.1017/S0263574719000602

A Study on Vibrations of Hexarot-Based High-G Centrifugal Simulators

Siamak Pedrammehr*, Houshyar Asadi and Saeid Nahavandi

Institute for Intelligent Systems Research and Innovation, Deakin University, Waurn Ponds Campus, Victoria 3216, Australia
E-mails: houshyar.asadi@deakin.edu.au, saeid.nahavandi@deakin.edu.au

(Accepted March 30, 2019. First published online: May 21, 2019)

SUMMARY
This paper investigates the vibrations of hexarot simulators. The generalized modeling of kinematics and dynamics formulation of a hexarot mechanism is addressed. This model considers the flexible manipulator with the base motion. The dynamic formulation has been developed based on the principle of virtual work. The dynamic model consists of the stiffness of the different parts of the mechanism, the effects of gravity and inertia, torque and force related to the joints viscous friction. Finally, the response of the end effector at various frequencies has been presented, and the vibrations of the mechanism and the dynamic stability index have been investigated.

KEYWORDS: Parallel mechanism; Hexarot; Simulator; Dynamics; Vibrations; Virtual work principle.

1. Introduction

Parallel manipulators have got a remarkable attention for several applications and especially as simulators. The vibration behavior and stability are among the demands for simulators. This needs a thoroughgoing understanding of the dynamics of the manipulator. The investigation that leads to gain the mentioned understanding is a necessary study issue that fills the existing gap in the reported researches in this respect.

The dynamics and vibrations of the parallel manipulators have been the aim of many studies in the reported literature to improve their efficiency. The closed-form dynamic formulation of parallel manipulators, which can be employed in vibration analysis of mechanism and its control system development, has mainly been developed in the reported literature following three methods, viz. Newton–Euler approach,[1–7] Euler–Lagrange approach,[7–12] and the principle of virtual work.[13–18] All the approaches that use classical mechanics result in equivalent dynamic formulations as they are describing the same manipulator; however, the obtained equations have different complexities and applications. For example, the Newton–Euler approach considers the internal forces and moments applied to different parts of the manipulator. This can be employed to the design of the manipulators. These internal forces and moments cannot be calculated, for example, by the principle of virtual work method. On the other hand, to solve the vibrations of the mechanism, the closed-form formulation is needed. The virtual work methodology gives the relationship between the different parts of the mechanism and its end effector. Lee and Geng,[19] and Selig and Ding[20] presented an analytical vibration model for a parallel mechanism. Yoshikawa[21] introduced manipulability to consider the manipulator's dynamic parameters. Ma and Angeles[22] proposed the dynamic conditioning index, and the optimum manipulator design considering the dynamic isotropy. Mukherjee et al.[23] studied the

* Corresponding author. E-mail: spedramm@deakin.edu.au, s.pedrammehr@gmail.com

https://doi.org/10.1017/S0263574719000602 Published online by Cambridge University Press

vibrations of a flexible Stewart mechanism and presented its dynamic stability index. The vibration theory has also been applied to model the parallel mechanisms and investigate their stability. Huang and Schimmels[24] considered flexibility of pods simply by assuming massless springs connected to the end effector as parallel pods. Hong et al.[25] have derived the vibration model of a parallel mechanism considering spring-damper systems and performed stability analysis. A flexible mechanism with spring-damper systems has also been considered for vibration analysis of hexapods, and the results are validated by experimental testing and finite element method (FEM).[26–28] Mahboubkhah et al.[29] also investigated the vibrations of a four-degrees of freedom (DOF) parallel mechanism using a finite element analysis. Afzali-Far et al.[30] studied damped vibrations of Stewart platforms and investigated the influence of inertia on its vibrations. The simplified dynamic formulation for hexarot coaxial parallel manipulators has been studied;[31–35] however, to the best of the authors' knowledge, no mathematical solutions exist for the dynamics and vibrations of the hexarots in the reported literature that consider all the effective parameters like the base motion, the stiffness of the different parts of the mechanism, the effects of gravity and inertia, and torque and force related to the joints viscous friction.

The following are the objectives of this study: developing a generalized closed-form dynamic formulation of hexarots consisting the stiffness of the different parts of the mechanism, and studying the effects of gravity and inertia, and torque and force related to the joints viscous friction. This formulation has been developed following the virtual work principle to investigate the vibrations of the hexarot manipulators. The rest of this paper is organized as follows: the hexarot mechanism is presented in Section 2. In Section 3, the generalized kinematic formulation, including the base motions, is developed. In Section 4, the generalized closed-form dynamic formulation of hexarot simulators is addressed. The linearization of the dynamic model is performed for vibration analysis in Section 5. Section 6 presents the simulation procedure under MATLAB conducted to investigate the linearized model. The FEM modal analysis has also been performed under ANSYS Workbench. Finally, the concluding remarks are given in Section 7.

2. Hexarot Mechanism[1]

Hexarots are the members of parallel simulation-based motion platform (SBMP) family that have recently been developed like the heaps of six DOF manipulators that are presented after the Stewart platform manipulator introduction.[36] Just like Stewart mechanisms these mechanisms are also known as flight simulators. However, hexarots are of interest as simulators with centrifugal high-G capabilities. There are noticeable differences between the hexarots and Stewart mechanisms that make their generated formulation and their mechanical analyses entirely different. In Stewart platforms the lower and upper links are aligned and joined with one DOF cylindrical joints; however, in hexarots, two DOF universal joints are used between the lower and upper links, and the links are not in the same direction. This, therefore, gives the completely different nature and formulation for the hexarots in comparison with the Stewart parallel kinematic manipulators. The location of the links on the base column significantly influences the kinematics and dynamics in hexarots, as well. In Stewart platforms, the forces needed for the linear elongation of the links are produced by the actuators.[5,6,37–39] However, the motors set at the base of hexarot mechanisms rotate the upper links. The moving parts' weight is reduced because of the active joint location. These active joints produce torques and provide the end effector motion. Limitless rotation possibility around the base column with coaxial actuators provides a very large workspace for hexarots that is not available in Stewart mechanisms.

The kinematics, workspace, error analysis, and control of the hexarot mechanism have then been studied in different research works.[40–43] Hexarot mechanism as a parallel manipulator using six 5 DOF passive arms to manipulate an end effector has several advantages. Five DOF arm is not sensitive to torsion or bending, and it is manufactured lightweight with a high stiffness. As the mechanism has six DOF of the manipulated end effector, mechanical redundancy will not exist. This, moreover, means that the arm system has a simple and precise assembly.[36] Hexarot axis-symmetric parallel mechanisms are a kind of parallel kinematic machines including an arm system with coaxial actuators and limitless capability of rotation about the central column. Almost all the parallel mechanisms suffer from a small workspace. However, the limitless capability of rotation about the central column

[1]Throughout this research, all parameters are in frame {**W**} except those indicated with upper prefix P and B.

https://doi.org/10.1017/S0263574719000602 Published online by Cambridge University Press

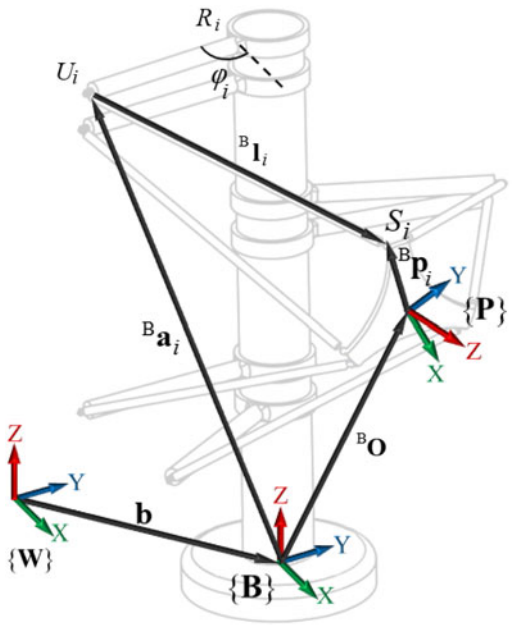


Fig. 1. Schematic view of hexarot simulator with frames and vector representation.

provides a considerably large workspace for the hexarots.[44] These mechanisms are mostly known as high-G centrifugal simulators.[31] The hexarot simulator has six DOF movements consisting of rotation and translation. This simulator has an end effector, six actuators and arms, and a central column (see Fig. 1). This mechanism's axis-symmetric property refers to the rotation axis of the actuators. Each of the arms includes two links: a lower link $\mathbf{l}_i$ and an upper link $\mathbf{a}_i$. Each upper link is respectively connected to the base column and the lower link through R_i rotational joint as actuators and the U_i universal joint. The end effector is connected to the other end of the lower link via S_i spherical joint. In order to model the mechanism, $\{\mathbf{W}\}$ is considered as a world frame. The frame $\{\mathbf{B}\}$ is attached to the mechanism's base. Furthermore, the frame $\{\mathbf{P}\}$ is fixed to the end effector. The characteristics of the simulator are listed in Appendix.

3. Generalized Kinematics

In order to develop dynamic equations, at first the kinematic relations of the links are studied. In this section, the kinematic relations for the moving parts of the manipulator including the base column motion are developed.

3.1. Kinematic relations in base frame of reference

Here, the relationship between the motion of the end effector and the links of the simulator with the reference in the frame $\{\mathbf{B}\}$ is obtained.

According to Fig. 1, the following relation can be written:

$$ {}^{B}\mathbf{a}_i + {}^{B}\mathbf{l}_i = {}^{B}\mathbf{O} + {}^{B}\mathbf{p}_i = {}^{B}\mathbf{O}_g + {}^{B}\mathbf{p}_i - {}^{B}\bar{\mathbf{r}} = {}^{B}\mathbf{O}_g + {}^{B}\bar{\mathbf{p}}_i \tag{1} $$

in which ${}^{B}\mathbf{a}_i$ and ${}^{B}\mathbf{p}_i$ are, respectively, the i^{th} universal and spherical joints' position vector in $\{\mathbf{B}\}$, ${}^{B}\mathbf{O}$ indicates the geometrical center of the end effector in $\{\mathbf{B}\}$ and ${}^{B}\mathbf{O}_g$ is the mass center of the end effector and payload in $\{\mathbf{B}\}$. ${}^{B}\bar{\mathbf{r}}$ is the vector for the mass center of the end effector in frame $\{\mathbf{B}\}$, and ${}^{B}\mathbf{l}_i$ is the lower link's length vector. ${}^{B}\bar{\mathbf{p}}_i$ is also considered equal to ${}^{B}\mathbf{p}_i - {}^{B}\bar{\mathbf{r}}$.

Taking the time derivative on both sides of Eq. (1) and taking the inner product of the resulting equation with ${}^{B}\hat{\mathbf{n}}_i$ as the unit vector along ${}^{B}\mathbf{l}_i$ gives:

$$ \varphi_i' \left({}^{B}\mathbf{a}_i \times {}^{B}\hat{\mathbf{n}}_i\right) \cdot {}^{B}\hat{\mathbf{Z}} = {}^{B}\mathbf{v}_{p/b} \cdot {}^{B}\hat{\mathbf{n}}_i + \left({}^{B}\mathbf{R}_{P}\, {}^{P}\mathbf{p}_i \times {}^{B}\hat{\mathbf{n}}_i\right) \cdot {}^{B}\boldsymbol{\omega}_{p/b} \tag{2} $$

where ${}^{P}\mathbf{p}_i$ is the i^{th} spherical joints' position vector in $\{\mathbf{P}\}$. ${}^{B}\mathbf{v}_{p/b}$ and ${}^{B}\boldsymbol{\omega}_{p/b}$ are, respectively, the linear and angular velocities of the end effector relative to the base frame. The angular velocity of the

https://doi.org/10.1017/S0263574719000602 Published online by Cambridge University Press

end effector in $\{\mathbf{B}\}$ can be obtained from the Euler angles' derivatives.[34] φ_i' is the angular velocity of the i^{th} actuated joint with ${}^{\mathrm{B}}\hat{\mathbf{Z}}$ as the unit vector along the Z axis of $\{\mathbf{B}\}$. ${}^{\mathrm{B}}\mathbf{R}_{\mathrm{P}}$ is the rotation matrix that maps between $\{\mathbf{P}\}$ and $\{\mathbf{B}\}$.[34]

By dividing two sides of Eq. (2) to $\left({}^{\mathrm{B}}\mathbf{a}_i \times {}^{\mathrm{B}}\hat{\mathbf{n}}_i\right) \cdot {}^{\mathrm{B}}\hat{\mathbf{Z}}$, the following is obtained:

$$\begin{bmatrix} \varphi_1' \\ \cdot \\ \cdot \\ \cdot \\ \varphi_6' \end{bmatrix} = \mathbf{J}_\varphi \begin{bmatrix} {}^{\mathrm{B}}\mathbf{v}_{p/b} \\ {}^{\mathrm{B}}\boldsymbol{\omega}_{p/b} \end{bmatrix} \tag{3}$$

where $\mathbf{J}_\varphi$ is called the Jacobian matrix of the end effector that relates the velocity of its mass center to the input joint velocities, and can be presented as:

$$\mathbf{J}_\varphi = \begin{bmatrix} \dfrac{{}^{\mathrm{B}}\hat{\mathbf{n}}_1^{\mathrm{T}}}{\left({}^{\mathrm{B}}\mathbf{a}_1 \times {}^{\mathrm{B}}\hat{\mathbf{n}}_1\right).{}^{\mathrm{B}}\hat{\mathbf{Z}}} & \dfrac{\left({}^{\mathrm{B}}\mathbf{R}_{\mathrm{P}}\,{}^{\mathrm{P}}\mathbf{p}_1 \times {}^{\mathrm{B}}\hat{\mathbf{n}}_1\right)^{\mathrm{T}}}{\left({}^{\mathrm{B}}\mathbf{a}_1 \times {}^{\mathrm{B}}\hat{\mathbf{n}}_1\right).{}^{\mathrm{B}}\hat{\mathbf{Z}}} \\ \vdots & \vdots \\ \dfrac{{}^{\mathrm{B}}\hat{\mathbf{n}}_6^{\mathrm{T}}}{\left({}^{\mathrm{B}}\mathbf{a}_6 \times {}^{\mathrm{B}}\hat{\mathbf{n}}_6\right).{}^{\mathrm{B}}\hat{\mathbf{Z}}} & \dfrac{\left({}^{\mathrm{B}}\mathbf{R}_{\mathrm{P}}\,{}^{\mathrm{P}}\mathbf{p}_6 \times {}^{\mathrm{B}}\hat{\mathbf{n}}_6\right)^{\mathrm{T}}}{\left({}^{\mathrm{B}}\mathbf{a}_6 \times {}^{\mathrm{B}}\hat{\mathbf{n}}_6\right).{}^{\mathrm{B}}\hat{\mathbf{Z}}} \end{bmatrix}_{6\times 6} \tag{4}$$

The distance between the i^{th} upper link's mass center and the corresponding actuator is indicated as r_{ai}, and ${}^{\mathrm{B}}\hat{\mathbf{c}}_i$ is the unit vector along the directions of each upper link. Thus, the velocity vector of the mass center of the i^{th} upper link with reference in frame $\{\mathbf{B}\}$ can be obtained as:

$${}^{\mathrm{B}}\mathbf{v}_{ai/b} = \varphi_i'\, r_{ai}\left({}^{\mathrm{B}}\hat{\mathbf{Z}} \times {}^{\mathrm{B}}\hat{\mathbf{c}}_i\right) \tag{5}$$

Substituting Eq. (2) into Eq. (5) gives:

$${}^{\mathrm{B}}\mathbf{v}_{ai/b} = r_{ai}\frac{\left({}^{\mathrm{B}}\hat{\mathbf{Z}} \times \hat{\mathbf{c}}_i\right)}{{}^{\mathrm{B}}\hat{\mathbf{Z}} \cdot \left({}^{\mathrm{B}}\mathbf{a}_i \times {}^{\mathrm{B}}\hat{\mathbf{n}}_i\right)}\left({}^{\mathrm{B}}\hat{\mathbf{n}}_i^{\mathrm{T}}\,{}^{\mathrm{B}}\mathbf{v}_{p/b} + \left({}^{\mathrm{B}}\mathbf{R}_{\mathrm{P}}\,{}^{\mathrm{P}}\mathbf{p}_i \times {}^{\mathrm{B}}\hat{\mathbf{n}}_i\right)^{\mathrm{T}}\,{}^{\mathrm{B}}\boldsymbol{\omega}_{p/b}\right) \tag{6}$$

Considering Eq. (2), the i^{th} upper link's angular velocity, ${}^{\mathrm{B}}\boldsymbol{\omega}_{ai/b}$, can be written in the base frame of reference as:

$${}^{\mathrm{B}}\boldsymbol{\omega}_{ai/b} = \varphi_i'{}^{\mathrm{B}}\hat{\mathbf{Z}} = {}^{\mathrm{B}}\hat{\mathbf{Z}}\frac{\left({}^{\mathrm{B}}\mathbf{v}_{p/b} \cdot {}^{B}\hat{\mathbf{n}}_i + {}^{\mathrm{B}}\boldsymbol{\omega}_{p/b} \cdot \left({}^{\mathrm{B}}\mathbf{R}_{\mathrm{p}}\,{}^{\mathrm{P}}\mathbf{p}_i \times {}^{\mathrm{B}}\hat{\mathbf{n}}_i\right)\right)}{{}^{\mathrm{B}}\hat{\mathbf{Z}} \cdot \left({}^{\mathrm{B}}\mathbf{a}_i \times {}^{\mathrm{B}}\hat{\mathbf{n}}_i\right)} \tag{7}$$

Combining Eqs. (6) and (7) the relation between the twist of the end effector and the twist of the upper links can be obtained as:

$$\begin{bmatrix} {}^{\mathrm{B}}\mathbf{v}_{ai/b} \\ {}^{\mathrm{B}}\boldsymbol{\omega}_{ai/b} \end{bmatrix} = \mathbf{J}_{ai} \begin{bmatrix} {}^{\mathrm{B}}\mathbf{v}_{p/b} \\ {}^{\mathrm{B}}\boldsymbol{\omega}_{p/b} \end{bmatrix} \tag{8}$$

where the Jacobian matrix that relates the motion of the end effector to the upper links $\mathbf{J}_{ai}$ is given as the following:

$$\mathbf{J}_{ai} = \begin{bmatrix} \dfrac{r_{ai}\left({}^{\mathrm{B}}\hat{\mathbf{Z}} \times {}^{\mathrm{B}}\mathbf{c}_i\right){}^{\mathrm{B}}\mathbf{n}_i^{\mathrm{T}}}{{}^{\mathrm{B}}\hat{\mathbf{Z}}\cdot\left({}^{\mathrm{B}}\mathbf{a}_i \times {}^{\mathrm{B}}\mathbf{n}_i\right)} & \dfrac{r_{ai}\left({}^{\mathrm{B}}\hat{\mathbf{Z}} \times {}^{\mathrm{B}}\mathbf{c}_i\right)\left({}^{\mathrm{B}}\mathbf{R}_{\mathrm{P}}\,{}^{\mathrm{P}}\mathbf{p}_i \times {}^{\mathrm{B}}\mathbf{n}_i\right)^{\mathrm{T}}}{{}^{\mathrm{B}}\hat{\mathbf{Z}}\cdot\left({}^{\mathrm{B}}\mathbf{a}_i \times {}^{\mathrm{B}}\mathbf{n}_i\right)} \\ \dfrac{{}^{\mathrm{B}}\hat{\mathbf{Z}}\,{}^{\mathrm{B}}\mathbf{n}_i^{\mathrm{T}}}{{}^{\mathrm{B}}\hat{\mathbf{Z}}\cdot\left({}^{\mathrm{B}}\mathbf{a}_i \times {}^{\mathrm{B}}\mathbf{n}_i\right)} & \dfrac{{}^{\mathrm{B}}\hat{\mathbf{Z}}\left({}^{\mathrm{B}}\mathbf{R}_{\mathrm{P}}\,{}^{\mathrm{P}}\mathbf{p}_i \times {}^{\mathrm{B}}\mathbf{n}_i\right)^{\mathrm{T}}}{{}^{\mathrm{B}}\hat{\mathbf{Z}}\cdot\left({}^{\mathrm{B}}\mathbf{a}_i \times {}^{\mathrm{B}}\mathbf{n}_i\right)} \end{bmatrix}_{6\times 6} \tag{9}$$

Considering the kinematics of universal joint of the hexarot, the unit vectors ${}^{\mathrm{B}}\hat{\mathbf{u}}_i$ and ${}^{\mathrm{B}}\hat{\mathbf{v}}_i$ indicate the joint's kinematic model. The unit vector ${}^{\mathrm{B}}\hat{\mathbf{u}}_i = {}^{\mathrm{B}}\hat{\mathbf{c}}_i$ is fixed to the upper link's joint axis, and ${}^{\mathrm{B}}\hat{\mathbf{v}}_i = {}^{\mathrm{B}}\hat{\mathbf{u}}_i \times {}^{\mathrm{B}}\hat{\mathbf{n}}_i \big/ \left|{}^{\mathrm{B}}\hat{\mathbf{u}}_i \times {}^{\mathrm{B}}\hat{\mathbf{n}}_i\right|$ is the unit vector perpendicular to ${}^{\mathrm{B}}\hat{\mathbf{u}}_i$ and ${}^{\mathrm{B}}\hat{\mathbf{n}}_i$.[34]

https://doi.org/10.1017/S0263574719000602 Published online by Cambridge University Press

Taking the time derivative on both sides of Eq. (1) and taking the cross product of both sides of the resulting equation with $\left({}^{\mathrm{B}}\hat{\mathbf{u}}_i \times {}^{\mathrm{B}}\hat{\mathbf{v}}_i\right)$ gives[2]:

$$\begin{aligned}&\left(\left({}^{\mathrm{B}}\hat{\mathbf{u}}_i \times {}^{\mathrm{B}}\hat{\mathbf{v}}_i\right) \cdot {}^{\mathrm{B}}\mathbf{l}_i\right) {}^{\mathrm{B}}\boldsymbol{\omega}_{li/b} - \left(\left({}^{\mathrm{B}}\hat{\mathbf{u}}_i \times {}^{\mathrm{B}}\hat{\mathbf{v}}_i\right) \cdot {}^{\mathrm{B}}\boldsymbol{\omega}_{li/b}\right) {}^{\mathrm{B}}\mathbf{l}_i = \\ &\left({}^{\mathrm{B}}\hat{\mathbf{u}}_i \times {}^{\mathrm{B}}\hat{\mathbf{v}}_i\right) \times {}^{\mathrm{B}}\mathbf{v}_{p/b} + \left(\left({}^{\mathrm{B}}\hat{\mathbf{u}}_i \times {}^{\mathrm{B}}\hat{\mathbf{v}}_i\right) \cdot \left({}^{\mathrm{B}}\mathbf{R}_{\mathrm{P}}\, {}^{\mathrm{P}}\mathbf{p}_i\right)\right) {}^{\mathrm{B}}\boldsymbol{\omega}_{p/b} - \\ &\left(\left({}^{\mathrm{B}}\hat{\mathbf{u}}_i \times {}^{\mathrm{B}}\hat{\mathbf{v}}_i\right) \cdot {}^{\mathrm{B}}\boldsymbol{\omega}_{p/b}\right) \left({}^{\mathrm{B}}\mathbf{R}_{\mathrm{P}}\, {}^{\mathrm{P}}\mathbf{p}_i\right) - \left({}^{\mathrm{B}}\hat{\mathbf{u}}_i \times {}^{\mathrm{B}}\hat{\mathbf{v}}_i\right) \times \left({}^{\mathrm{B}}\boldsymbol{\omega}_{ai/b} \times {}^{\mathrm{B}}\mathbf{a}_i\right)\end{aligned} \tag{10}$$

in which ${}^{\mathrm{B}}\boldsymbol{\omega}_{li/b}$ is the i^{th} lower link's angular velocity in $\{\mathbf{B}\}$.

Since $\left({}^{\mathrm{B}}\hat{\mathbf{u}}_i \times {}^{\mathrm{B}}\hat{\mathbf{v}}_i\right) \cdot {}^{\mathrm{B}}\boldsymbol{\omega}_{li/b} = 0$, Eq. (10) can be simplified to[3]:

$$\begin{aligned}&\left(\left({}^{\mathrm{B}}\hat{\mathbf{u}}_i \times {}^{\mathrm{B}}\hat{\mathbf{v}}_i\right) \cdot {}^{\mathrm{B}}\mathbf{l}_i\right) {}^{\mathrm{B}}\boldsymbol{\omega}_{li/b} = \\ &\left(\left(\left({}^{\mathrm{B}}\hat{\mathbf{u}}_i \times {}^{\mathrm{B}}\hat{\mathbf{v}}_i\right)^{\mathrm{T}} \left({}^{\mathrm{B}}\mathbf{R}_{\mathrm{P}}\, {}^{\mathrm{P}}\mathbf{p}_i\right)\right) \mathbf{1}_{3\times 3} - \left(\left({}^{\mathrm{B}}\mathbf{R}_{\mathrm{P}}\, {}^{\mathrm{P}}\mathbf{p}_i\right) \left({}^{\mathrm{B}}\hat{\mathbf{u}}_i \times {}^{\mathrm{B}}\hat{\mathbf{v}}_i\right)^{\mathrm{T}}\right)_{3\times 3}\right) {}^{\mathrm{B}}\boldsymbol{\omega}_{p/b} \\ &+ \left[{}^{\mathrm{B}}\hat{\mathbf{u}}_i \times {}^{\mathrm{B}}\hat{\mathbf{v}}_i\right]_{\times} {}^{\mathrm{B}}\mathbf{v}_{p/b} - \left({}^{\mathrm{B}}\hat{\mathbf{u}}_i \times {}^{\mathrm{B}}\hat{\mathbf{v}}_i\right) \times \left({}^{\mathrm{B}}\boldsymbol{\omega}_{ai/b} \times {}^{\mathrm{B}}\mathbf{a}_i\right)\end{aligned} \tag{11}$$

where $\mathbf{1}_{3\times 3}$ is 3×3 identity matrix, and $[\mathbf{a}]_{\times}$[4] denotes the skew-symmetric of its vector argument, viz $\mathbf{a}$, which is usually used for conversion of a cross product to a matrix multiplication.

Substituting φ_i' from Eq. (2) into Eq. (11), the i^{th} lower link's angular velocity can be obtained in the matrix form as [5]:

$${}^{\mathrm{B}}\boldsymbol{\omega}_{li/b} = \begin{bmatrix}\boldsymbol{\Gamma}_i & \boldsymbol{\Lambda}_i\end{bmatrix} \begin{bmatrix}{}^{\mathrm{B}}\mathbf{v}_{p/b} \\ {}^{\mathrm{B}}\boldsymbol{\omega}_{p/b}\end{bmatrix} \tag{12}$$

where

$$\boldsymbol{\Gamma}_i = \frac{{}^{\mathrm{B}}\hat{\mathbf{v}}_i\, {}^{\mathrm{B}}\hat{\mathbf{u}}_i^{\mathrm{T}} - {}^{\mathrm{B}}\hat{\mathbf{u}}_i\, {}^{\mathrm{B}}\hat{\mathbf{v}}_i^{\mathrm{T}}}{\left({}^{\mathrm{B}}\hat{\mathbf{u}}_i \times {}^{\mathrm{B}}\hat{\mathbf{v}}_i\right) \cdot {}^{\mathrm{B}}\mathbf{l}_i} - \frac{\left({}^{\mathrm{B}}\hat{\mathbf{u}}_i \times {}^{\mathrm{B}}\hat{\mathbf{v}}_i\right) \times \left({}^{\mathrm{B}}\hat{\mathbf{Z}} \times {}^{\mathrm{B}}\mathbf{a}_i\right) {}^{\mathrm{B}}\hat{\mathbf{n}}_i^{\mathrm{T}}}{\left(\left({}^{\mathrm{B}}\hat{\mathbf{u}}_i \times {}^{\mathrm{B}}\hat{\mathbf{v}}_i\right) \cdot {}^{\mathrm{B}}\mathbf{l}_i\right) \left({}^{\mathrm{B}}\hat{\mathbf{Z}} \cdot \left({}^{\mathrm{B}}\mathbf{a}_i \times {}^{\mathrm{B}}\hat{\mathbf{n}}_i\right)\right)} \tag{13}$$

$$\begin{aligned}\boldsymbol{\Lambda}_i = &\frac{\left({}^{\mathrm{B}}\hat{\mathbf{u}}_i \times {}^{\mathrm{B}}\hat{\mathbf{v}}_i\right)^{\mathrm{T}} \left({}^{\mathrm{B}}\mathbf{R}_{\mathrm{P}}\, {}^{\mathrm{P}}\mathbf{p}_i\right) \mathbf{1}_{3\times 3} - \left({}^{\mathrm{B}}\mathbf{R}_{\mathrm{P}}\, {}^{\mathrm{P}}\mathbf{p}_i\right) \left({}^{\mathrm{B}}\hat{\mathbf{u}}_i \times {}^{\mathrm{B}}\hat{\mathbf{v}}_i\right)^{\mathrm{T}}}{\left({}^{\mathrm{B}}\hat{\mathbf{u}}_i \times {}^{\mathrm{B}}\hat{\mathbf{v}}_i\right) \cdot {}^{\mathrm{B}}\mathbf{l}_i} \\ &- \frac{\left(\left({}^{\mathrm{B}}\hat{\mathbf{u}}_i \times {}^{\mathrm{B}}\hat{\mathbf{v}}_i\right) \times \left({}^{\mathrm{B}}\hat{\mathbf{Z}} \times {}^{\mathrm{B}}\mathbf{a}_i\right)\right) \left(\left({}^{\mathrm{B}}\mathbf{R}_{\mathrm{P}}\, {}^{\mathrm{P}}\mathbf{p}_i\right) \times {}^{\mathrm{B}}\hat{\mathbf{n}}_i\right)^{\mathrm{T}}}{\left(\left({}^{\mathrm{B}}\hat{\mathbf{u}}_i \times {}^{\mathrm{B}}\hat{\mathbf{v}}_i\right) \cdot {}^{\mathrm{B}}\mathbf{l}_i\right) \left({}^{\mathrm{B}}\hat{\mathbf{Z}} \cdot \left({}^{\mathrm{B}}\mathbf{a}_i \times {}^{\mathrm{B}}\hat{\mathbf{n}}_i\right)\right)}\end{aligned} \tag{14}$$

The distance between the i^{th} lower link's mass center and its corresponding universal joint is indicated as r_{li}. Therefore, the velocity vector of the mass center of the i^{th} lower link with reference in frame $\{\mathbf{B}\}$ can be obtained as:

$${}^{\mathrm{B}}\mathbf{v}_{li/b} = {}^{\mathrm{B}}\boldsymbol{\omega}_{ai/b} \times {}^{\mathrm{B}}\mathbf{a}_i + r_{li}\, {}^{\mathrm{B}}\boldsymbol{\omega}_{li/b} \times {}^{\mathrm{B}}\hat{\mathbf{n}}_i \tag{15}$$

Substituting φ_i' from Eq. (2) into Eq. (15), the i^{th} lower link's linear velocity can be obtained as:

$${}^{\mathrm{B}}\mathbf{v}_{li/b} = \begin{bmatrix}\boldsymbol{\Xi}_i & \boldsymbol{\Psi}_i\end{bmatrix} \begin{bmatrix}{}^{\mathrm{B}}\mathbf{v}_{p/b} \\ {}^{\mathrm{B}}\boldsymbol{\omega}_{p/b}\end{bmatrix} \tag{16}$$

[2]The rule $\mathbf{a} \times (\mathbf{b} \times \mathbf{c}) = (\mathbf{a} \cdot \mathbf{c})\ \mathbf{b} - (\mathbf{a} \cdot \mathbf{b})\ \mathbf{c}$ is used.

[3]The rule $\mathbf{a} \cdot \mathbf{b} = \mathbf{a}^{\mathrm{T}}\mathbf{b}$ is used.

[4] $[\mathbf{a}]_{\times} = \begin{bmatrix}0 & -a_z & a_y \\ a_z & 0 & -a_x \\ -a_y & a_x & 0\end{bmatrix}$

[5]The relation $[\mathbf{a} \times \mathbf{b}]_{\times} = \mathbf{b}\mathbf{a}^{\mathrm{T}} - \mathbf{a}\mathbf{b}^{\mathrm{T}}$ is used.

https://doi.org/10.1017/S0263574719000602 Published online by Cambridge University Press

where

$$\boldsymbol{\Xi}_i = \frac{\left({}^{\mathrm{B}}\hat{\mathbf{Z}} \times {}^{\mathrm{B}}\mathbf{a}_i\right) {}^{\mathrm{B}}\hat{\mathbf{n}}_i^{\mathrm{T}}}{{}^{\mathrm{B}}\hat{\mathbf{Z}} \cdot \left({}^{\mathrm{B}}\mathbf{a}_i \times {}^{\mathrm{B}}\hat{\mathbf{n}}_i\right)} - r_{li} \left[{}^{\mathrm{B}}\hat{\mathbf{n}}_i\right]_{\times} \boldsymbol{\Gamma}_i \tag{17}$$

$$\boldsymbol{\Psi}_i = \frac{\left({}^{\mathrm{B}}\hat{\mathbf{Z}} \times {}^{\mathrm{B}}\mathbf{a}_i\right) \left(\left({}^{\mathrm{B}}\mathbf{R}_{\mathrm{P}} {}^{\mathrm{P}}\mathbf{p}_i\right) \times {}^{\mathrm{B}}\hat{\mathbf{n}}_i\right)^{\mathrm{T}}}{{}^{\mathrm{B}}\hat{\mathbf{Z}} \cdot \left({}^{\mathrm{B}}\mathbf{a}_i \times {}^{\mathrm{B}}\hat{\mathbf{n}}_i\right)} - r_{li} \left[{}^{\mathrm{B}}\hat{\mathbf{n}}_i\right]_{\times} \boldsymbol{\Lambda}_i \tag{18}$$

Combining Eqs. (12) and (16) gives the relation between the twist of the end effector and the twist of the lower link:

$$\begin{bmatrix} {}^{\mathrm{B}}\mathbf{v}_{li/b} \\ {}^{\mathrm{B}}\boldsymbol{\omega}_{li/b} \end{bmatrix} = \mathbf{J}_{li} \begin{bmatrix} {}^{\mathrm{B}}\mathbf{v}_{p/b} \\ {}^{\mathrm{B}}\boldsymbol{\omega}_{p/b} \end{bmatrix} \tag{19}$$

Therefore, the Jacobian matrix that relates the motion of the end effector to the lower links $\mathbf{J}_{li}$ is given as the following:

$$\mathbf{J}_{li} = \begin{bmatrix} \boldsymbol{\Xi}_i & \boldsymbol{\Psi}_i \\ \boldsymbol{\Gamma}_i & \boldsymbol{\Lambda}_i \end{bmatrix} \tag{20}$$

3.2. Kinematic relations considering the base motion

In the previous section, the Jacobians between the end effector and the links of the simulator are obtained in the base frame of reference. Here, in this section, the generalized kinematic relations are obtained considering the motion of the central base column.

Referring to Fig. 1, the linear and angular velocities of the i^{th} upper link can be obtained in world frame as the following:

$$\mathbf{v}_{ai} = \mathbf{v}_b + \boldsymbol{\omega}_b \times \left({}^{\mathrm{W}}\mathbf{R}_{\mathrm{B}} \left(r_{ai} {}^{\mathrm{B}}\hat{\mathbf{c}}_i + h_i {}^{\mathrm{B}}\hat{\mathbf{Z}}\right)\right) + {}^{\mathrm{W}}\mathbf{R}_{\mathrm{B}} {}^{\mathrm{B}}\mathbf{v}_{ai/b} \tag{21}$$

$$\boldsymbol{\omega}_{ai} = \boldsymbol{\omega}_b + {}^{\mathrm{W}}\mathbf{R}_{\mathrm{B}} {}^{\mathrm{B}}\boldsymbol{\omega}_{ai/b} \tag{22}$$

in which the mapping between $\{\mathbf{B}\}$ and $\{\mathbf{W}\}$ is achieved through ${}^{\mathrm{W}}\mathbf{R}_{\mathrm{B}}$ rotation matrix. $\mathbf{v}_b$ and $\boldsymbol{\omega}_b$ are, respectively, the linear and angular velocities of the base relative to the world coordinate frame. $\mathbf{v}_{ai}$ and $\boldsymbol{\omega}_{ai}$ are, respectively, the linear and angular velocities of the i^{th} upper link relative to the world coordinate frame. h_i is also the height of each universal joint.

Combining Eqs. (21) and (22) gives the following closed-form equation:

$$\begin{bmatrix} \mathbf{v}_{ai} \\ \boldsymbol{\omega}_{ai} \end{bmatrix} = \begin{bmatrix} \mathbf{1}_{3\times 3} & -\left[{}^{\mathrm{W}}\mathbf{R}_{\mathrm{B}} \left(r_{ai} {}^{\mathrm{B}}\hat{\mathbf{c}}_i + h_i {}^{\mathrm{B}}\hat{\mathbf{Z}}\right)\right]_{\times} \\ \mathbf{0}_{3\times 3} & \mathbf{1}_{3\times 3} \end{bmatrix} \begin{bmatrix} \mathbf{v}_b \\ \boldsymbol{\omega}_b \end{bmatrix} + \begin{bmatrix} {}^{\mathrm{W}}\mathbf{R}_{\mathrm{B}} & \mathbf{0}_{3\times 3} \\ \mathbf{0}_{3\times 3} & {}^{\mathrm{W}}\mathbf{R}_{\mathrm{B}} \end{bmatrix} \begin{bmatrix} {}^{\mathrm{B}}\mathbf{v}_{ai/b} \\ {}^{\mathrm{B}}\boldsymbol{\omega}_{ai/b} \end{bmatrix} \tag{23}$$

where $\mathbf{0}_{3\times 3}$ is 3×3 zero matrix.

Substituting Eq. (8) into Eq. (23) yields:

$$\begin{bmatrix} \mathbf{v}_{ai} \\ \boldsymbol{\omega}_{ai} \end{bmatrix} = \mathbf{Q}_{ai} \begin{bmatrix} \mathbf{v}_b \\ \boldsymbol{\omega}_b \end{bmatrix} + \bar{\mathbf{J}}_{ai} \begin{bmatrix} {}^{\mathrm{B}}\mathbf{v}_{p/b} \\ {}^{\mathrm{B}}\boldsymbol{\omega}_{p/b} \end{bmatrix} \tag{24}$$

where $\mathbf{Q}_{ai}$ and $\bar{\mathbf{J}}_{ai}$ are as follows:

$$\mathbf{Q}_{ai} = \begin{bmatrix} \mathbf{1}_{3\times 3} & -\left[{}^{\mathrm{W}}\mathbf{R}_{\mathrm{B}} \left(r_{ai} {}^{\mathrm{B}}\hat{\mathbf{c}}_i + h_i {}^{\mathrm{B}}\hat{\mathbf{Z}}\right)\right]_{\times} \\ \mathbf{0}_{3\times 3} & \mathbf{1}_{3\times 3} \end{bmatrix} \tag{25}$$

$$\bar{\mathbf{J}}_{ai} = \begin{bmatrix} {}^{\mathrm{W}}\mathbf{R}_{\mathrm{B}} & \mathbf{0}_{3\times 3} \\ \mathbf{0}_{3\times 3} & {}^{\mathrm{W}}\mathbf{R}_{\mathrm{B}} \end{bmatrix} \mathbf{J}_{ai} \tag{26}$$

https://doi.org/10.1017/S0263574719000602 Published online by Cambridge University Press

By using a similar procedure, the closed-form velocity equation of the i^{th} lower link can be obtained in world frame of reference as the following:

$$\begin{bmatrix} \mathbf{v}_{li} \\ \boldsymbol{\omega}_{li} \end{bmatrix} = \mathbf{Q}_{li} \begin{bmatrix} \mathbf{v}_b \\ \boldsymbol{\omega}_b \end{bmatrix} + \bar{\mathbf{J}}_{li} \begin{bmatrix} {}^{\mathrm{B}}\mathbf{v}_{p/b} \\ {}^{\mathrm{B}}\boldsymbol{\omega}_{p/b} \end{bmatrix} \tag{27}$$

in which $\mathbf{v}_{li}$ and $\boldsymbol{\omega}_{li}$ are, respectively, the linear and angular velocities of the i^{th} lower link relative to the world frame of reference. $\mathbf{Q}_{li}$ and $\bar{\mathbf{J}}_{li}$ are also defined as the following:

$$\mathbf{Q}_{li} = \begin{bmatrix} \mathbf{1}_{3\times 3} & -\left[{}^{\mathrm{W}}\mathbf{R}_{\mathrm{B}}\left(r_{li}{}^{\mathrm{B}}\hat{\mathbf{n}}_i + {}^{\mathrm{B}}\mathbf{a}_i\right)\right]_{\times} \\ \mathbf{0}_{3\times 3} & \mathbf{1}_{3\times 3} \end{bmatrix} \tag{28}$$

$$\bar{\mathbf{J}}_{li} = \begin{bmatrix} {}^{\mathrm{W}}\mathbf{R}_{\mathrm{B}} & \mathbf{0}_{3\times 3} \\ \mathbf{0}_{3\times 3} & {}^{\mathrm{W}}\mathbf{R}_{\mathrm{B}} \end{bmatrix} \mathbf{J}_{li} \tag{29}$$

The closed-form velocity equation of the end effector can similarly be obtained in world frame of reference as the following:

$$\begin{bmatrix} \mathbf{v}_p \\ \boldsymbol{\omega}_p \end{bmatrix} = \mathbf{Q}_p \begin{bmatrix} \mathbf{v}_b \\ \boldsymbol{\omega}_b \end{bmatrix} + \bar{\mathbf{J}}_p \begin{bmatrix} {}^{\mathrm{B}}\mathbf{v}_{p/b} \\ {}^{\mathrm{B}}\boldsymbol{\omega}_{p/b} \end{bmatrix} \tag{30}$$

$\mathbf{Q}_p$ and $\bar{\mathbf{J}}_p$ are also defined as the following:

$$\mathbf{Q}_p = \begin{bmatrix} \mathbf{1}_{3\times 3} & -\left[{}^{\mathrm{W}}\mathbf{R}_{\mathrm{B}}\,{}^{\mathrm{B}}\mathbf{O}\right]_{\times} \\ \mathbf{0}_{3\times 3} & \mathbf{1}_{3\times 3} \end{bmatrix} \tag{31}$$

$$\bar{\mathbf{J}}_p = \begin{bmatrix} {}^{\mathrm{W}}\mathbf{R}_{\mathrm{B}} & \mathbf{0}_{3\times 3} \\ \mathbf{0}_{3\times 3} & {}^{\mathrm{W}}\mathbf{R}_{\mathrm{B}} \end{bmatrix} \tag{32}$$

4. Generalized Closed-Form Dynamics

The generalized dynamic modeling of the hexarot simulator is developed through the virtual work principle. In the d'Alembert's form of the virtual work, unlike the Newton–Euler and Lagrangian methods, there is no need to open the understudy manipulator to an equal tree structure mechanism, and contain the constraint relations because of the joints' cut. Base motions, friction in both the passive and active joints, and flexibility of the upper links are taken into the consideration, in this section.

4.1. Applied and inertia wrenches

Considering the d'Alembert's principle, the force exerted at the mass center of each body consists of the inertial force and the gravity force. The moment acting on each rigid body is also the inertial moment. The resultant of applied and inertia wrenches applied to the reference point of the end effector, and i^{th} upper and lower links, that is, $\mathbf{F}_p$, $\mathbf{F}_{ai}$, and $\mathbf{F}_{li}$, can, respectively, be written as:

$$\begin{aligned} \mathbf{F}_p &= \begin{bmatrix} \mathbf{F}_{\text{ext}} + m_p\left(\mathbf{G} - \mathbf{v}'_p\right) \\ \mathbf{M}_{\text{ext}} - \sum_{i=1}^{6} C_{Si}\left(\boldsymbol{\omega}_{p/b} - \boldsymbol{\omega}_{li/b}\right) - \boldsymbol{\omega}_p \times \left(\mathbf{I}_p\boldsymbol{\omega}_p\right) - \mathbf{I}_p\boldsymbol{\omega}'_p \end{bmatrix} \\ &= \begin{bmatrix} \mathbf{F}_{\text{ext}} \\ \mathbf{M}_{\text{ext}} \end{bmatrix} + \begin{bmatrix} m_p\mathbf{G} \\ -\sum_{i=1}^{6} C_{Si}\left(\boldsymbol{\omega}_{p/b} - \boldsymbol{\omega}_{li/b}\right) - \boldsymbol{\omega}_p \times \left(\mathbf{I}_p\boldsymbol{\omega}_p\right) \end{bmatrix} - \begin{bmatrix} m_p\mathbf{1}_{3\times 3} & \mathbf{0}_{3\times 3} \\ \mathbf{0}_{3\times 3} & {}^{\mathrm{W}}\mathbf{I}_p \end{bmatrix} \begin{bmatrix} \mathbf{v}'_p \\ \boldsymbol{\omega}'_p \end{bmatrix} \end{aligned} \tag{33}$$

$$\begin{aligned} \mathbf{F}_{ai} &= \begin{bmatrix} m_{ai}\left(\mathbf{G} - \mathbf{v}'_{ai}\right) \\ C_{Ui}\left(\boldsymbol{\omega}_{li/b} - \boldsymbol{\omega}_{ai/b}\right) - \boldsymbol{\omega}_{ai} \times \mathbf{I}_{ai}\boldsymbol{\omega}_{ai}) - \mathbf{I}_{ai}\boldsymbol{\omega}'_{ai} \end{bmatrix} \\ &= \begin{bmatrix} m_{ai}\mathbf{G} \\ C_{Ui}\left(\boldsymbol{\omega}_{li/b} - \boldsymbol{\omega}_{ai/b}\right) - {}^{\mathrm{W}}\boldsymbol{\omega}_{ai} \times \left(\mathbf{I}_{ai}\boldsymbol{\omega}_{ai}\right) \end{bmatrix} - \begin{bmatrix} m_{ai}\mathbf{1}_{3\times 3} & \mathbf{0}_{3\times 3} \\ \mathbf{0}_{3\times 3} & {}^{\mathrm{W}}\mathbf{I}_{ai} \end{bmatrix} \begin{bmatrix} \mathbf{v}'_{ai} \\ \boldsymbol{\omega}'_{ai} \end{bmatrix} \end{aligned} \tag{34}$$

https://doi.org/10.1017/S0263574719000602 Published online by Cambridge University Press

$$\begin{aligned}\mathbf{F}_{li} &= \begin{bmatrix} m_{li}\left(\mathbf{G}-\mathbf{v}'_{li}\right) \\ C_{Si}\left(\boldsymbol{\omega}_{p/b}-\boldsymbol{\omega}_{li/b}\right)-C_{Ui}\left(\boldsymbol{\omega}_{li/b}-\boldsymbol{\omega}_{ai/b}\right)-\boldsymbol{\omega}_{li}\times\left(\mathbf{I}_{li}\boldsymbol{\omega}_{li}\right)-\mathbf{I}_{li}\boldsymbol{\omega}'_{li}\end{bmatrix} \\ &= \begin{bmatrix} m_{li}\mathbf{G} \\ C_{Si}\left(\boldsymbol{\omega}_{p/b}-\boldsymbol{\omega}_{li}\right)-C_{Ui}\left(\boldsymbol{\omega}_{li/b}-\boldsymbol{\omega}_{ai/b}\right)-\boldsymbol{\omega}_{li}\times\left(\mathbf{I}_{li}\boldsymbol{\omega}_{li}\right)\end{bmatrix}-\begin{bmatrix} m_{li}\mathbf{1}_{3\times 3} & \mathbf{0}_{3\times 3} \\ \mathbf{0}_{3\times 3} & {}^{\mathrm{W}}\mathbf{I}_{li}\end{bmatrix}\begin{bmatrix}\mathbf{v}'_{li}\\ \boldsymbol{\omega}'_{li}\end{bmatrix}\end{aligned} \tag{35}$$

where $\mathbf{v}'_p$, $\mathbf{v}'_{ai}$, and $\mathbf{v}'_{li}$ are the acceleration vectors of the mass centers of the end effector, the i^{th} upper link, and i^{th} lower link in frame $\{\mathbf{W}\}$, respectively. $\mathbf{I}_p = {}^{\mathrm{W}}\mathbf{R}_{\mathrm{P}}{}^{\mathrm{P}}\mathbf{I}_p{}^{\mathrm{W}}\mathbf{R}_{\mathrm{P}}^{\mathrm{T}}$, $\mathbf{I}_{ai} = {}^{\mathrm{W}}\mathbf{R}_{ai}{}^{ai}\mathbf{I}_{ai}{}^{\mathrm{W}}\mathbf{R}_{ai}^{\mathrm{T}}$, and $\mathbf{I}_{li} = {}^{\mathrm{W}}\mathbf{R}_{li}{}^{li}\mathbf{I}_{li}{}^{\mathrm{W}}\mathbf{R}_{li}^{\mathrm{T}}$ are, respectively, the inertia tensor of the end effector, the i^{th} upper link, and i^{th} lower link in $\{\mathbf{W}\}$ as well. ${}^{\mathrm{P}}\mathbf{I}_p$, ${}^{ai}\mathbf{I}_{ai}$, and ${}^{li}\mathbf{I}_{li}$ are also the inertia tensor of the end effector, the i^{th} upper and lower links expressed relative to their local frame of reference, that is, their center of mass. The viscous friction coefficient of the i^{th} universal and spherical joints is, respectively, denoted by C_{Ui} and C_{Si}. $\mathbf{F}_{\text{ext}}$ and $\mathbf{M}_{\text{ext}}$ are also the external force and moment acting on the origin of the end effector.

4.2. Dynamic model

According to the virtual work principle, dynamics of the understudy manipulator can be expressed as:

$$\delta\boldsymbol{\varphi}^{\mathrm{T}}\boldsymbol{\tau}+\sum_{i=1}^{6}\delta\boldsymbol{\mathcal{X}}_{ai}^{\mathrm{T}}\mathbf{F}_{ai}+\sum_{i=1}^{6}\delta\boldsymbol{\mathcal{X}}_{li}^{\mathrm{T}}\mathbf{F}_{li}+\delta\boldsymbol{\mathcal{X}}_{p}^{\mathrm{T}}\mathbf{F}_{p}+\delta\boldsymbol{\mathcal{X}}_{b}^{\mathrm{T}}\mathbf{F}_{b}=0 \tag{36}$$

where $\delta\boldsymbol{\varphi}$ is the vector of virtual displacements of the actuated joints and $\delta\boldsymbol{\mathcal{X}}_{ai}$, $\delta\boldsymbol{\mathcal{X}}_{li}$, $\delta\boldsymbol{\mathcal{X}}_{p}$, and $\delta\boldsymbol{\mathcal{X}}_{b}$ are, respectively, the virtual twists of the end effector, i^{th} upper link, i^{th} lower link, and the base. $\mathbf{F}_b$ is also the wrench applied to the base column, and $\boldsymbol{\tau}$ is the actuator torques dependent on the type of the actuators and can be defined as:

$$\boldsymbol{\tau}=\begin{bmatrix}\tau_1-C_{A1}\varphi' \\ \cdot \\ \cdot \\ \cdot \\ \tau_6-C_{A6}\varphi'_6\end{bmatrix} \tag{37}$$

in which τ_i and C_{Ai} are, respectively, the torque and the viscous friction coefficient of the i^{th} actuator.

Considering the manipulator Jacobian matrix in Eqs. (4), (24), (27), and (30), $\delta\boldsymbol{\varphi}$, $\delta\boldsymbol{\mathcal{X}}_{ai}$, $\delta\boldsymbol{\mathcal{X}}_{li}$, and $\delta\boldsymbol{\mathcal{X}}_{p}$ can be obtained in terms of the virtual twist of the base, that is, $\delta\boldsymbol{\mathcal{X}}_{b}$, and the virtual twist of the end effector relative to the base frame, that is, $\delta\boldsymbol{\mathcal{X}}_{p/b}$, as:

$$\delta\boldsymbol{\varphi}=\mathbf{J}_{\varphi}\delta\boldsymbol{\mathcal{X}}_{p/b} \tag{38}$$

$$\delta\boldsymbol{\mathcal{X}}_{p}=\mathbf{Q}_{p}\delta\boldsymbol{\mathcal{X}}_{b}+\bar{\mathbf{J}}_{p}\delta\boldsymbol{\mathcal{X}}_{p/b} \tag{39}$$

$$\delta\boldsymbol{\mathcal{X}}_{ai}=\mathbf{Q}_{ai}\delta\boldsymbol{\mathcal{X}}_{b}+\bar{\mathbf{J}}_{ai}\delta\boldsymbol{\mathcal{X}}_{p/b} \tag{40}$$

$$\delta\boldsymbol{\mathcal{X}}_{li}=\mathbf{Q}_{li}\delta\boldsymbol{\mathcal{X}}_{b}+\bar{\mathbf{J}}_{li}\delta\boldsymbol{\mathcal{X}}_{p/b} \tag{41}$$

Substituting Eqs. (38)–(41) into Eq. (36) yields:

$$\delta\boldsymbol{\mathcal{X}}_{p/b}^{\mathrm{T}}\left(\mathbf{J}_{\varphi}^{\mathrm{T}}\boldsymbol{\tau}+\sum_{i=1}^{6}\bar{\mathbf{J}}_{ai}^{\mathrm{T}}\mathbf{F}_{ai}+\sum_{i=1}^{6}\bar{\mathbf{J}}_{li}^{\mathrm{T}}\mathbf{F}_{li}+\bar{\mathbf{J}}_{p}^{\mathrm{T}}\mathbf{F}_{p}\right)+\delta\boldsymbol{\mathcal{X}}_{b}^{\mathrm{T}}\left(\mathbf{F}_{b}+\sum_{i=1}^{6}\mathbf{Q}_{ai}^{\mathrm{T}}\mathbf{F}_{ai}+\sum_{i=1}^{6}\mathbf{Q}_{li}^{\mathrm{T}}\mathbf{F}_{li}+\mathbf{Q}_{p}^{\mathrm{T}}\mathbf{F}_{p}\right)=0 \tag{42}$$

Since Eq. (42) holds for any $\delta\boldsymbol{\mathcal{X}}_{p/b}^{\mathrm{T}}$ and $\delta\boldsymbol{\mathcal{X}}_{b}^{\mathrm{T}}$, we have:

$$\mathbf{J}_{\varphi}^{\mathrm{T}}\boldsymbol{\tau}+\sum_{i=1}^{6}\bar{\mathbf{J}}_{ai}^{\mathrm{T}}\mathbf{F}_{ai}+\sum_{i=1}^{6}\bar{\mathbf{J}}_{li}^{\mathrm{T}}\mathbf{F}_{li}+\bar{\mathbf{J}}_{p}^{\mathrm{T}}\mathbf{F}_{p}=0 \tag{43}$$

$$\mathbf{F}_{b}+\sum_{i=1}^{6}\mathbf{Q}_{ai}^{\mathrm{T}}\mathbf{F}_{ai}+\sum_{i=1}^{6}\mathbf{Q}_{li}^{\mathrm{T}}\mathbf{F}_{li}+\mathbf{Q}_{p}^{\mathrm{T}}\mathbf{F}_{p}=0 \tag{44}$$

https://doi.org/10.1017/S0263574719000602 Published online by Cambridge University Press

As we do not intend to obtain the force and moment exerted to the base column, that is, $\mathbf{F}_b$, we will refer Eq. (43) as the dynamic model of the manipulator for the rest of the paper.

Substituting Eqs. (33)–(35) into Eq. (43) and using Eqs. (24), (27), and (30), gives:

$$\mathcal{M}\begin{bmatrix} {}^{\mathrm{B}}\mathbf{v}'_{p/b} \\ {}^{\mathrm{B}}\boldsymbol{\omega}'_{p/b} \end{bmatrix} + \mathcal{N}\begin{bmatrix} \mathbf{v}'_b \\ \boldsymbol{\omega}'_b \end{bmatrix} + \mathcal{C} = \mathbf{J}_\varphi^{\mathrm{T}}\boldsymbol{\tau} + \bar{\mathbf{J}}_p^{\mathrm{T}}\begin{bmatrix} \mathbf{F}_{\mathrm{ext}} \\ \mathbf{M}_{\mathrm{ext}} \end{bmatrix} \tag{45}$$

where

$$\mathcal{M} = \bar{\mathbf{J}}_p^{\mathrm{T}}\begin{bmatrix} m_p\mathbf{1}_{3\times3} & \mathbf{0}_{3\times3} \\ \mathbf{0}_{3\times3} & \mathbf{I}_p \end{bmatrix}\bar{\mathbf{J}}_p + \sum_{i=1}^{6}\bar{\mathbf{J}}_{ai}^{\mathrm{T}}\begin{bmatrix} m_{ai}\mathbf{1}_{3\times3} & \mathbf{0}_{3\times3} \\ \mathbf{0}_{3\times3} & \mathbf{I}_{ai} \end{bmatrix}\bar{\mathbf{J}}_{ai} + \bar{\mathbf{J}}_{li}^{\mathrm{T}}\begin{bmatrix} m_{li}\mathbf{1}_{3\times3} & \mathbf{0}_{3\times3} \\ \mathbf{0}_{3\times3} & \mathbf{I}_{li} \end{bmatrix}\bar{\mathbf{J}}_{li} \tag{46}$$

$$\mathcal{N} = \bar{\mathbf{J}}_p^{\mathrm{T}}\begin{bmatrix} m_p\mathbf{1}_{3\times3} & \mathbf{0}_{3\times3} \\ \mathbf{0}_{3\times3} & \mathbf{I}_p \end{bmatrix}\mathbf{Q}_p + \sum_{i=1}^{6}\bar{\mathbf{J}}_{ai}^{\mathrm{T}}\begin{bmatrix} m_{ai}\mathbf{1}_{3\times3} & \mathbf{0}_{3\times3} \\ \mathbf{0}_{3\times3} & \mathbf{I}_{ai} \end{bmatrix}\mathbf{Q}_{ai} + \bar{\mathbf{J}}_{li}^{\mathrm{T}}\begin{bmatrix} m_{li}\mathbf{1}_{3\times3} & \mathbf{0}_{3\times3} \\ \mathbf{0}_{3\times3} & \mathbf{I}_{li} \end{bmatrix}\mathbf{Q}_{li} \tag{47}$$

$$\begin{aligned} \mathcal{C} = {} & \mathcal{C}_p\begin{bmatrix} {}^{\mathrm{B}}\mathbf{v}_{p/b} \\ {}^{\mathrm{B}}\boldsymbol{\omega}_{p/b} \end{bmatrix} + \mathcal{C}_b\begin{bmatrix} \mathbf{v}_b \\ \boldsymbol{\omega}_b \end{bmatrix} - \bar{\mathbf{J}}_p^{\mathrm{T}}\begin{bmatrix} m_p\mathbf{G} \\ -\sum_{i=1}^{6} C_{Si}\left(\boldsymbol{\omega}_{p/b} - \boldsymbol{\omega}_{li/b}\right) - \boldsymbol{\omega}_p \times (\mathbf{I}_p\boldsymbol{\omega}_p) \end{bmatrix} \\ & - \sum_{i=1}^{6}\bar{\mathbf{J}}_{ai}^{\mathrm{T}}\begin{bmatrix} m_{ai}\mathbf{G} \\ C_{Ui}\left(\boldsymbol{\omega}_{li/b} - \boldsymbol{\omega}_{ai/b}\right) - \boldsymbol{\omega}_{ai} \times (\mathbf{I}_{ai}\boldsymbol{\omega}_{ai}) \end{bmatrix} \\ & + \bar{\mathbf{J}}_{li}^{\mathrm{T}}\begin{bmatrix} m_{li}\mathbf{G} \\ C_{Si}\left(\boldsymbol{\omega}_{p/b} - \boldsymbol{\omega}_{li/b}\right) - C_{Ui}\left(\boldsymbol{\omega}_{li/b} - \boldsymbol{\omega}_{ai/b}\right) - \boldsymbol{\omega}_{li} \times (\mathbf{I}_{li}\boldsymbol{\omega}_{li}) \end{bmatrix} \end{aligned} \tag{48}$$

in which

$$\mathcal{C}_p = \bar{\mathbf{J}}_p^{\mathrm{T}}\begin{bmatrix} m_p\mathbf{1}_{3\times3} & \mathbf{0}_{3\times3} \\ \mathbf{0}_{3\times3} & \mathbf{I}_p \end{bmatrix}\bar{\mathbf{J}}'_p + \sum_{i=1}^{6}\bar{\mathbf{J}}_{ai}^{\mathrm{T}}\begin{bmatrix} m_{ai}\mathbf{1}_{3\times3} & \mathbf{0}_{3\times3} \\ \mathbf{0}_{3\times3} & \mathbf{I}_{ai} \end{bmatrix}\bar{\mathbf{J}}'_{ai} + \bar{\mathbf{J}}_{li}^{\mathrm{T}}\begin{bmatrix} m_{li}\mathbf{1}_{3\times3} & \mathbf{0}_{3\times3} \\ \mathbf{0}_{3\times3} & \mathbf{I}_{li} \end{bmatrix}\bar{\mathbf{J}}'_{li} \tag{49}$$

$$\mathcal{C}_b = \bar{\mathbf{J}}_p^{\mathrm{T}}\begin{bmatrix} m_p\mathbf{1}_{3\times3} & \mathbf{0}_{3\times3} \\ \mathbf{0}_{3\times3} & \mathbf{I}_p \end{bmatrix}\mathbf{Q}'_p + \sum_{i=1}^{6}\bar{\mathbf{J}}_{ai}^{\mathrm{T}}\begin{bmatrix} m_{ai}\mathbf{1}_{3\times3} & \mathbf{0}_{3\times3} \\ \mathbf{0}_{3\times3} & \mathbf{I}_{ai} \end{bmatrix}\mathbf{Q}'_{ai} + \bar{\mathbf{J}}_{li}^{\mathrm{T}}\begin{bmatrix} m_{li}\mathbf{1}_{3\times3} & \mathbf{0}_{3\times3} \\ \mathbf{0}_{3\times3} & \mathbf{I}_{li} \end{bmatrix}Q'_{li} \tag{50}$$

5. Vibration Analysis

Here only the response of the end effector to the initial disturbances is of interest. Therefore, the external loads and the base column motion can be assumed to be zero. Considering Eq. (45), the dynamic closed-form relation of the hexarot in the joint space can be written as:

$$\mathbf{J}_\varphi^{-\mathrm{T}}\mathcal{M}\,\mathbf{J}_\varphi^{-1}\,\boldsymbol{\varphi}'' + \mathbf{J}_\varphi^{-\mathrm{T}}\left(\mathcal{C} - \mathcal{M}\mathbf{J}_\varphi^{-1}\mathbf{q}\right) = \boldsymbol{\tau} \tag{51}$$

in which

$$\mathbf{q} = \mathbf{J}'_\varphi\begin{bmatrix} {}^{\mathrm{B}}\mathbf{v}_{p/b} \\ {}^{\mathrm{B}}\boldsymbol{\omega}_{p/b} \end{bmatrix} \tag{52}$$

In general, there are several parameters that influence the stiffness of a simulator mechanism such as material and size of the links, the actuators types, gearboxes, and the control algorithm. However, considering that the manipulator links are thick enough and stiff, we can assume that only the actuators and gearboxes are the main sources of compliance in the manipulator.[45–51] Hence, the magnitude of the i^{th} actuator torque can be obtained for vibration analysis as the following:

$$\tau_i = -K_i\left(\varphi_i - \varphi_{i,0}\right) = -K_i\Delta\varphi_i \tag{53}$$

where $\varphi_{i,0}$ is the equilibrium angle of the i^{th} actuator, and K_i is the torsional stiffness of the joint. For free vibration analysis of the simulator, $\mathcal{C}$ and $\mathbf{q}$ in Eq. (51) are taken out of account.[7,52] Hence, combining Eqs. (51) and (53) gives:

$$\mathbf{J}_\varphi^{-\mathrm{T}}\,\mathcal{M}\,\mathbf{J}_\varphi^{-1}\,\boldsymbol{\varphi}'' = -\mathbf{K}\left(\boldsymbol{\varphi} - \boldsymbol{\varphi}_0\right) \tag{54}$$

https://doi.org/10.1017/S0263574719000602 Published online by Cambridge University Press

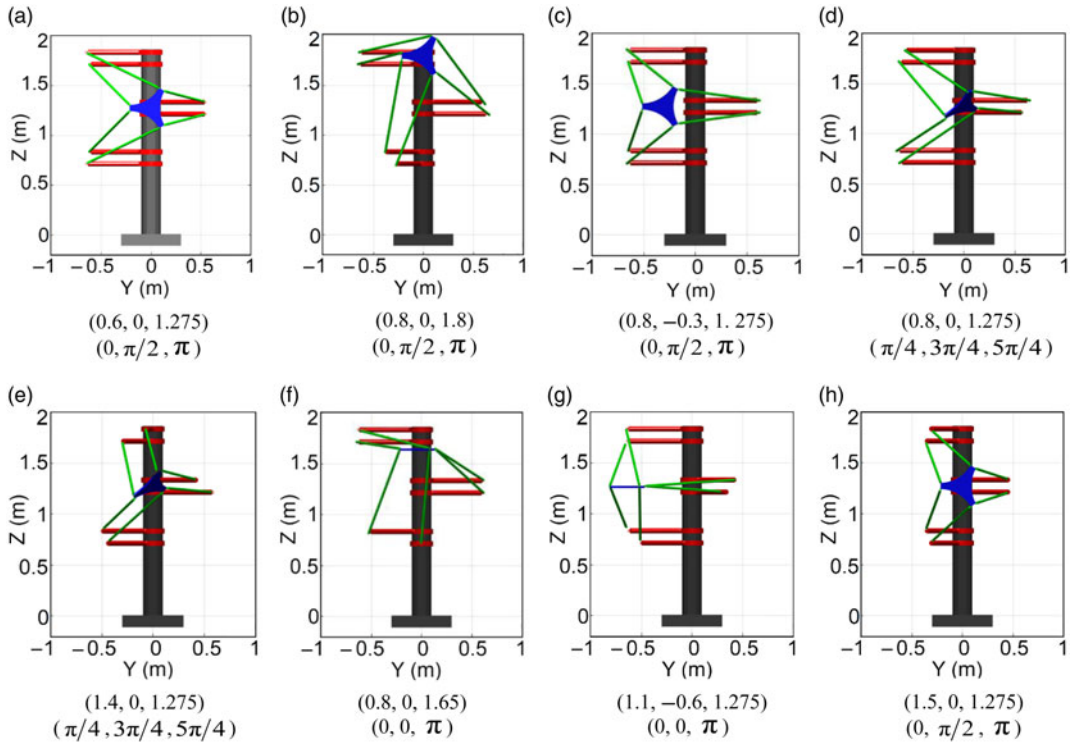


Fig. 2. Different configurations of end effector within the workspace borders.

where $\mathbf{K} = \text{diag}\,(K_i)$ is the stiffness matrix. Here $\mathbf{J}_\varphi$ and $\boldsymbol{\mathcal{M}}$ both depend on the constant properties of the simulator and the pose of the end effector. Therefore, the mode shapes and natural frequencies of the manipulator are dependent on the configuration of the end effector. For a particular configuration, $\mathbf{J}_\varphi$ and $\boldsymbol{\mathcal{M}}$ are constant. Therefore, $\mathbf{J}_\varphi^{-\mathrm{T}}\,\boldsymbol{\mathcal{M}}\,\mathbf{J}_\varphi^{-1}$ will be constant for that configuration.

Considering Eq. (3) and $\boldsymbol{\varphi}_s e^{i\omega t}$ as its solution, the generalized eigenvalue problem can be written as the following:

$$\omega^2 \left(\mathbf{J}_\varphi^{-\mathrm{T}}\,\boldsymbol{\mathcal{M}}\,\mathbf{J}_\varphi^{-1}\right) \boldsymbol{\varphi}_s = K\boldsymbol{\varphi}_s \tag{55}$$

By solving Eq. (55), six mode shapes and six natural frequencies for any particular configuration of the hexarot simulator can be obtained.

6. Simulation Study

In order to demonstrate the results of the developed generalized closed-form dynamic formulation and the linearized model, the case studies are performed in this section. For this purpose, the generalized eigenvalue problem of Eq. (55) is solved using a written code for the dynamics and vibration of hexarot simulator under MATLAB software. Upon the change in the configuration of the mechanism that leads to change in mass and stiffness matrices, the mode shapes and related natural frequencies vary.[53] Throughout the problem-solving procedure, eight different configurations of mechanism are selected (see Fig. 2). The natural frequencies of the mechanism are obtained by the analytical approach, and the results are listed in Table I for each position and orientation of the end effector shown in Fig. 2. According to the obtained results, configuration (a) in Fig. 2 exhibits the highest frequencies of the mechanism.

To corroborate the results, the natural frequencies of the end effector are also obtained by using FEM modal analysis for a specific configuration of Fig. 2a. To this end, a three-dimensional model of hexarot that has been developed in SolidWorks, exported to ANSYS Workbench, and the necessary input data such as material properties have been applied. The model elements have been made under Solid element. This model has 34,847 elements and 69,051 nodes. Finally, the modal analysis has been performed to obtain the natural frequencies and mode shapes of the end effector.

https://doi.org/10.1017/S0263574719000602 Published online by Cambridge University Press

Table I. Natural frequencies (rad/s) obtained by the analytical approach.

Configurations (Fig. 2)	**a**	**b**	**c**	**d**	**e**	**f**	**g**	**h**
1st Mode	72.8	74.9	52.7	29.1	23.9	22.2	36.0	56.5
2nd Mode	97.4	82.7	86.9	82.1	62.8	90.4	78.0	64.5
3rd Mode	113.5	100.2	98.5	97.6	76.2	100.5	79.5	91.6
4th Mode	116.8	103.3	101.9	102.0	97.6	113.5	87.4	110.3
5th Mode	118.6	119.3	107.5	108.9	119.6	119.7	105.6	116.0
6th Mode	120.2	128.4	109.2	111.5	131.7	135.0	111.6	120.4

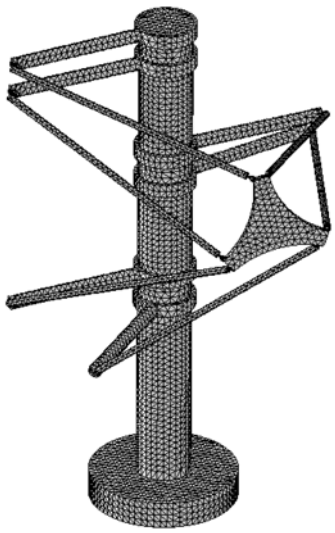


Fig. 3. The discretized model of understudy hexarot.

When we perform a modal analysis, we find eigenvalues (the frequencies), and eigenmodes associated to these frequencies (the deformed shapes). Mode shapes provide the most prominent deflection contributors for generalized (nonspecific) loading. The discretized model in the ANSYS Workbench is shown in Fig. 3. In this study, ANSYS Workbench has been used to examine the natural frequencies obtained by the solution of the eigenvalue problem for just one specific configuration of the mechanism.

It is important to note that the FEM frequencies are noticeable by the mode shapes for each configuration of the mechanism. In Fig. 4, the mode shapes are presented for the configuration $\mathbf{O} = [0.6\ 0\ 1.275]^{\mathrm{T}}$ and $\boldsymbol{\theta} = \left[0\ \pi/2\ \pi\right]^{\mathrm{T}}$.

The vibration simulation is performed for two sets of design parameters of hexarot simulator. The first case study is simulated for a general hexarot mechanism,[31–35] and the second case is a simulator that is designed for minimum condition number of Jacobian matrix $\mathbf{J}_{\varphi}$.[31] Figure 5 depicts the change in the least natural frequency with the change in the condition number of $\mathbf{J}_{\varphi}$ for different payloads. The values of the design parameters of both the cases are provided in Appendix.

According to Fig. 5, it is clear that the first natural frequency of hexarot reduces when the condition number of $\mathbf{J}_{\varphi}$ increases. The first natural frequency's low value also denotes the instability of the end effector. In different configurations of the end effector, the pattern in the plots between the dynamic and the static indices is clear, which gives the correlation between the dynamic stability and the Jacobian matrix's condition number.

Per Fig. 5(b) and 5(d), the different payload mass on the end effector leads to change in the lowest natural frequency of mechanism with the same kinematic parameters. In both cases, the first natural frequency declines when the mass of the end effector and the payload increases. This, however, signifies decreasing the dynamic stability of the end effector. In addition, since the condition number of $\mathbf{J}_{\varphi}$ does not depend on dynamic parameters, it cannot support the mentioned result.

https://doi.org/10.1017/S0263574719000602 Published online by Cambridge University Press

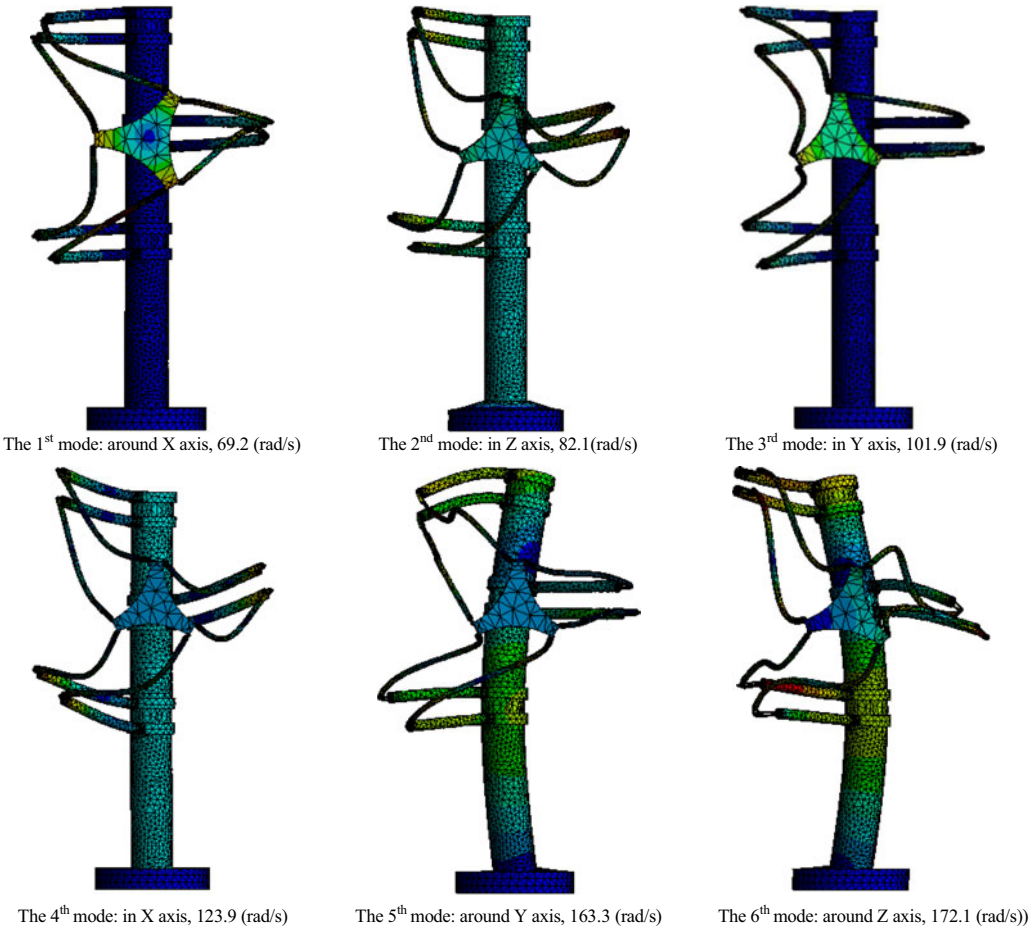


Fig. 4. Vibration modes of hexarot with $\mathbf{O} = [0.6\ 0\ 1.275]^{\mathrm{T}}$ and $\boldsymbol{\theta} = [0\ \pi/2\ \pi]^{\mathrm{T}}$.

The linearization of the dynamic model given in Eq. (54) is corroborated by simulations of the dynamic equation given in Eq. (45).

Numerical simulation is used to solve the movement of the end effector for a given base column motion, as there is no available analytic approach to solve the problem. Considering state variables as position, orientation, linear, and angular velocities of the end effector, Eq. (45) can be expressed in state-space as:

$$\mathcal{Z}' = \begin{bmatrix} \mathcal{Z}\,(7:12) \\ \mathcal{M}^{-1}\left(\mathbf{J}_{\varphi}^{\mathrm{T}}\boldsymbol{\tau} + \bar{\mathbf{J}}_{p}^{\mathrm{T}}\begin{bmatrix}\mathbf{F}_{\mathrm{ext}} \\ \mathbf{M}_{\mathrm{ext}}\end{bmatrix} - \mathcal{N}\begin{bmatrix}\mathbf{v}_b' \\ \boldsymbol{\omega}_b'\end{bmatrix} - \mathcal{C}\right) \end{bmatrix} \tag{56}$$

where $\mathcal{Z}$ is the state vector and $\mathcal{Z}'$ can be obtained as:

$$\mathcal{Z}' = \begin{bmatrix} {}^{\mathrm{W}}\mathbf{v}_{p/b}' \\ {}^{\mathrm{W}}\boldsymbol{\omega}_{p/b}' \\ {}^{\mathrm{W}}\mathbf{v}_{p/b} \\ {}^{\mathrm{W}}\boldsymbol{\omega}_{p/b} \end{bmatrix} \tag{57}$$

Considering the design parameters of Case 1 given in Appendix, Eq. (56) has been solved for the hexarot simulator under MATLAB software. In this simulation, the base column is subjected to x-directional excitations with 10^{-4} (m) amplitude at different frequencies. It is assumed that the end effector is in its reference position and orientation, that is, $\left[0.8\ 0\ 1.5\right]$ and $\left[0\ \pi/2\ \pi\right]$, at the equilibrium point. Two different natures of responses of the end effector are illustrated; one condition

https://doi.org/10.1017/S0263574719000602 Published online by Cambridge University Press

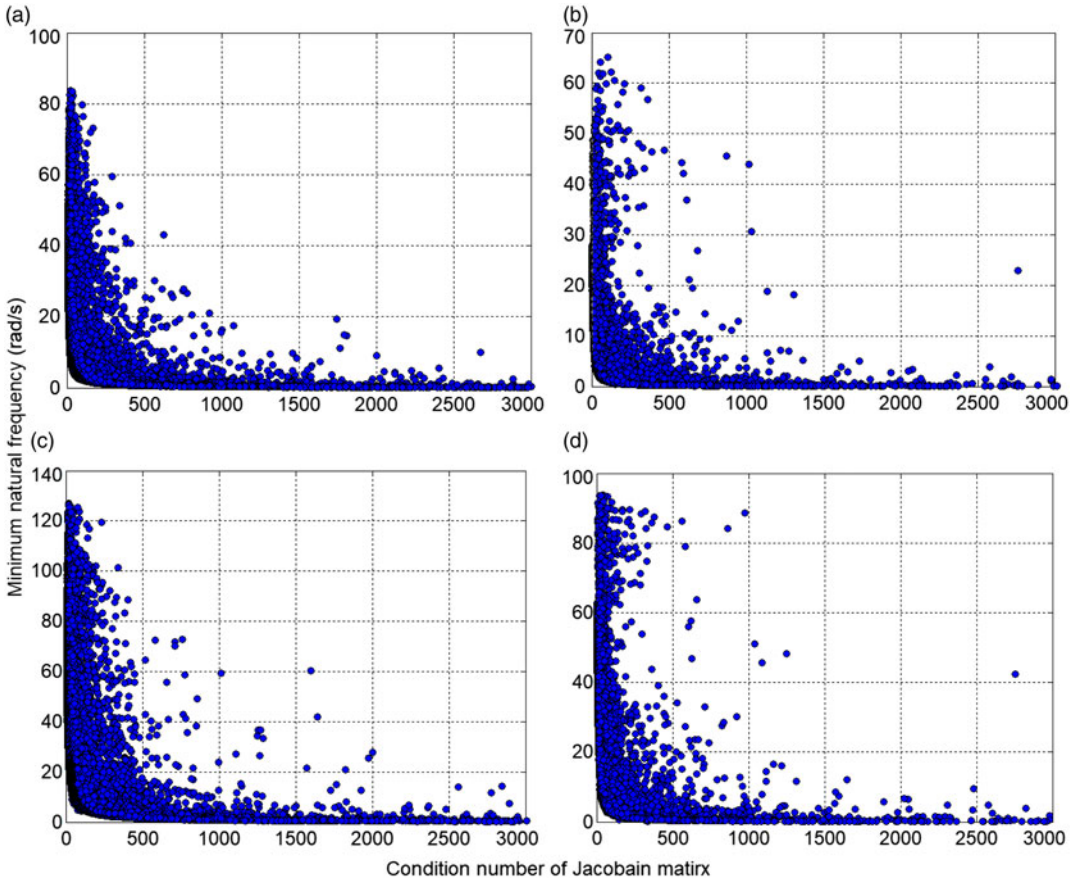


Fig. 5. Variation of minimum natural frequency with the change in the condition number of $\mathbf{J}_{\varphi}$: (a) Case 1, $m_p = 5.76$ (kg); (b) Case 1, $m_{p+payload} = 57.6$ (kg); (c) Case 2, $m_p = 17$ (kg); and (d) Case 2, $m_{p+payload} = 170$ (kg).

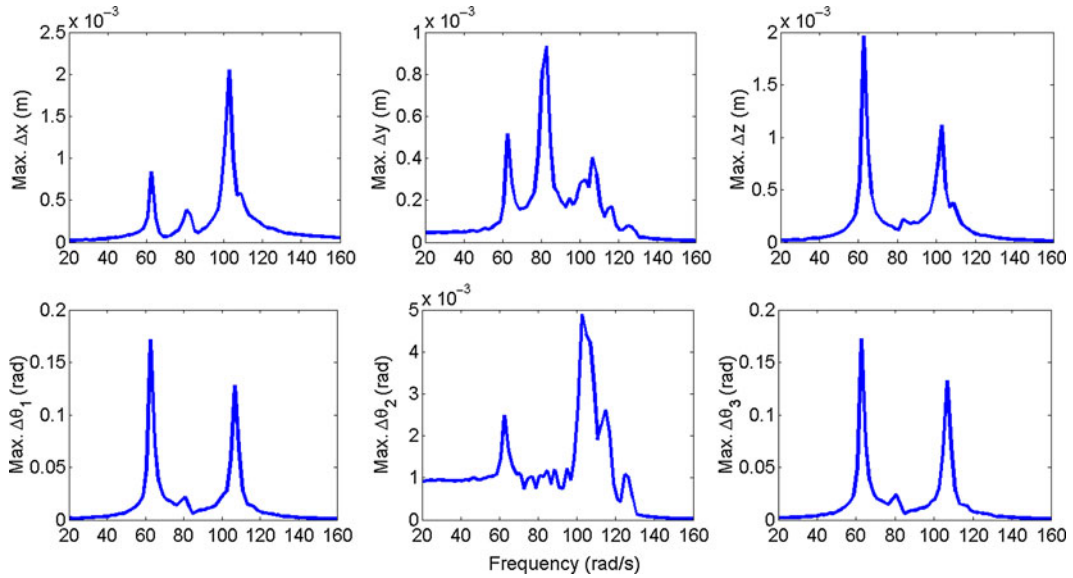


Fig. 6. The response of the end effector to the excitation of the base.

is that the excitation frequency is equal or close to the natural frequencies of the end effector, and the other is the condition that the excitation frequency is away from them.

Figure 6 depicts the response amplitude of the mechanism against the excitation frequency of the base for the different base excitations. Per the mathematical model, it is quite apparent that the

https://doi.org/10.1017/S0263574719000602 Published online by Cambridge University Press

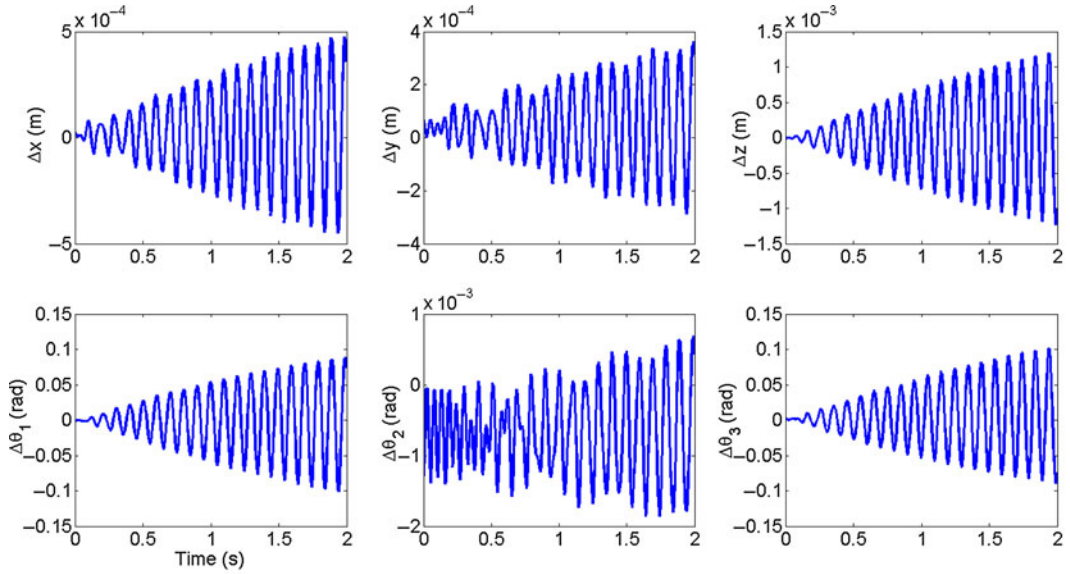


Fig. 7. Vibrations of the end effector in different directions at the excitation frequency of $\omega = 64.36$ (rad/s), equal to the first natural frequency.

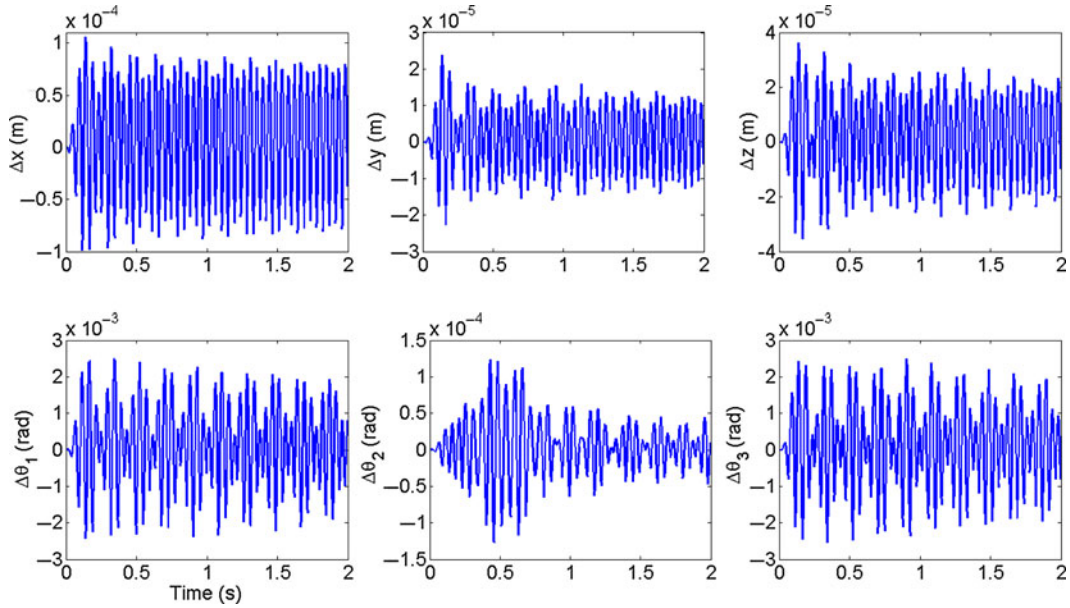


Fig. 8. Vibrations of the end effector in different directions at the excitation frequency of $\omega = 140$ (rad/s), away from the natural frequencies of the mechanism.

understudy simulator mechanism has six natural frequencies. Figure 6 represents that the hexarot manipulator resonates when the excitation is close to the natural frequencies obtained by the linearized model. Figure 7 indicates a typical response plot of the end effector at the first natural frequency. The responses of the end effector to the base excitations with a frequency away from the natural frequencies of the mechanism are also illustrated in Fig. 8.

7. Conclusions

In this research, a generalized formulation of the dynamics of a hexarot mechanism was developed through the virtual work approach. The mechanism stiffness, inertia and mass of base and arms, gravitation, base motion, and joints friction were taken into account. This model, moreover, can be utilized for control system development and design methodology purposes. The simulations were performed to investigate the dynamic model linearization and obtained natural frequencies. The

https://doi.org/10.1017/S0263574719000602 Published online by Cambridge University Press

obtained simulation results show that the mechanism will resonate and become unstable at the natural frequencies. Therefore, these frequencies should be considered and avoided in design and control of the simulator. The results also show that if the least natural frequency is small, the manipulator is likely to be unstable.

The main contributions and concluding remarks per the obtained results are as follows:

1. Mathematical dynamic model based on the D'Alembert's form is developed for hexarots. The developed model considers all the stiffness, gravity and inertia, joints friction.
2. A generalized closed-form formulation is obtained, and linearized for vibration analysis. This vibration model is quite economic in terms of the number of equations.
3. The theoretical model has been simulated under the code written in MATLAB for the vibrations of hexarot mechanism.
4. The change in the configuration of the mechanism that leads to change in mass and stiffness matrices, the mode shapes, and related natural frequencies varies. The reference configuration exhibits the highest frequencies of the mechanism, and the least natural frequencies are obtained when there are maximum changes in the orientation of the end effector.
5. One of the design criteria for optimizing the dynamic stability of the hexarot simulator that should be taken into consideration is to maximize the least natural frequency.
6. The natural frequencies play a prominent role in selecting the gains for the development of control system. This should be considered in a way that the simulator closed-loop poles do not become equal or close to the natural frequencies. If this happens, the considerable vibrations will occur in the controlled mechanism.
7. The range of natural frequencies helps to estimate the sampling time Δt for the control system. To have a proper control, Δt should be considered at most as $\Delta t = 2\pi / 20\, \omega_{n\max}$, in which $\omega_{n\max}$ is the highest natural frequency.

References

1. W. Q. D. Do and D. C. H. Yang, "Inverse dynamic analysis and simulation of a platform type of robot," *J. Robot Syst.* 5, 209–227 (1998).
2. S. Riebe and H. Ulbrich, "Modeling and online computation of the dynamics of a parallel kinematic with six degrees-of freedom," *Arch. Appl. Mech.* 72, 81–829 (2003).
3. A. Rahmani, A. Ghanbari, and S. Pedrammehr, "Kinematic analysis for hybrid 2-(6-UPU) manipulator by wavelet neural network," *Adv. Mater. Res.* 1016, 726–730 (2014).
4. W. Khalil and S. Guega, "Inverse and direct dynamic modeling of Gough-Stewart robots," *IEEE Trans. Rob.* 20, 755–761 (2004).
5. S. Pedrammehr, M. Mahboubkhah, and S. Pakzad, "An improved solution to the inverse dynamics of the general Stewart platform," *2011 IEEE International Conference on Mechatronics (ICM)*, Istanbul, Turkey (2011) pp. 392–397.
6. S. Pedrammehr, M. Mahboubkhah, and N. Khani, "Improved dynamic equations for the generally configured Stewart platform manipulator," *J. Mech. Sci. Technol.* 26, 711–721 (2012).
7. S. N. Yurt, E. Anli, and I. Ozkol, "On the characterization of the dynamic performances of planar manipulators," *Meccanica* 42, 187–196 (2007).
8. Y. Ting, Y. S. Chen, and H. C. Jar, "Modeling and control for a Gough-Stewart platform CNC machine," *J. Field Rob.* 21, 609–623 (2004).
9. Z. Geng, L. S. Haynes, T. D. Lee, and R. L. Carroll, "On the dynamic and kinematic analysis of a class of Stewart platform," *Rob. Autonom. Syst.* 9, 237–254 (1992).
10. S. S. Lee and J. M. Lee, "Design of a general purpose 6-DOF haptic interface," *Mechatronics* 13, 697–722 (2003).
11. G. Lebret, K. Liu, and F. L. Lewis, "Dynamic analysis and control of a Stewart Platform manipulator," *J. Robotic. Syst.* 10, 629–655 (1993).
12. W. Wang, H. Y. Yang, J. Zou, X. D. Ruan, and X. Fu, "Optimal design of Stewart platforms based on expanding the control bandwidth while considering the hydraulic system design," *J. Zhejiang Univ. Sci. A* 10, 22–30 (2009).
13. J. Wang and C. M. Gosselin, "A new approach for the dynamic analysis of parallel manipulators," *Multibody Syst. Dyn.* 2, 317–334 (1998).
14. C. D. Zhang and S. M. Song, "An efficient method for inverse dynamics of manipulators based on the virtual work principle," *J. Rob. Syst.* 10, 605–627 (1993).
15. R. D. Gregorio and V. Parenti-Castelli, "On the characterization of the dynamic performances of planar manipulators," *Meccanica* 40, 267–279 (2005).
16. L. W. Tsai, "Solving the inverse dynamics of a Stewart-Gough manipulator by the principle of virtual work," *J. Mech. Des.* 122, 3–9 (2000).
17. M. H. Abedinnasab and G. R. Vossoughi, "Analysis of a 6-DOF redundantly actuated 4-legged parallel mechanism," *Nonlinear Dyn.* 58, 611–622 (2009).

https://doi.org/10.1017/S0263574719000602 Published online by Cambridge University Press

18. Y. Zhao and F. Gao, "Inverse dynamics of the 6-dof out-parallel manipulator by means of the principle of virtual work," *Robotica* 27, 259–268 (2009).
19. J. D. Lee and J. Z. Geng, "A dynamic model of a flexible Stewart platform," *Comput. Struct.* 48, 367–374 (1993).
20. J. M. Selig and X. Ding, "Theory of vibration in Stewart platform," *Proceedings of the IEEE International Conference on Intelligent Robots and Systems*, Maui, Hawaii, USA (2001) pp. 2190–2195.
21. T. Yoshikawa, "Dynamic manipulability of robot manipulators," *IEEE Conference on Decision and Control,* St. Louis, MO, USA (1985) Vol. 2, pp. 1033–1038.
22. O. Ma and J. Angeles, "Optimum design of manipulator under dynamic isotropy condition," *Proceedings of the IEEE International Conference on Robotics and Automation*, (1993) Vol. 1, pp. 470–475
23. P. Mukherjee, B. Dasgupta, and A. K. Mallik, "Dynamic stability index and vibration analysis of a flexible Stewart platform," *J. Sound Vib.* 307, 495–512 (2007).
24. S. Huang and M. Schimmels, "The bounds and realization of spatial stiffnesses achieved with simple springs connected in parallel," *IEEE Trans. Robot. Autom.* 14, 466–475 (1998).
25. D. Hong, S. Kim, W. C. Choi, and J.-B. Song, "Analysis of machining stability for a parallel machine tool," *Mech. Base Des. Struct. Mach.* 31, 509–528 (2003).
26. S. Pedrammehr, M. Mahboubkhah, and N. Khani, "Natural frequencies and mode shapes for vibrations of machine tools' hexapod table," *1st International Conference on Acoustics and Vibration ISAV 2011*, Tehran, Iran (2011).
27. S. Pedrammehr, M. Mahboubkhah, M. R. C. Qazani, A. Rahmani, and S. Pakzad, "Forced vibration analysis of milling machines hexapod table under machining forces," *Stroj Vestn-J. Mech. E* 60, 158–171 (2014).
28. S. Pedrammehr, "Investigation of factors influential on the dynamic features of machine tools' hexapod table," *2nd International Conference on Acoustics and Vibration ISAV 2012*, Tehran, Iran (2012).
29. M. Mahboubkhah, S. Pakzad, A. G. Arasi, and M. M. Ettefagh, "Modal analysis of the vertical moving table of 4-DOF parallel machine tool by FEM and experimental test," *J. Vibro Eng.* 19, 7 (2017).
30. B. Afzali-Far, P. Lidström, and K. Nilsson, "Parametric damped vibrations of Gough-Stewart platforms for symmetric configurations," *Mech. Mach. Theory* 80, 52–69 (2014).
31. S. Pedrammehr, Z. Najdovski, H. Abdi, and S. Nahavandi, "Design methodology for a hexarot-based centrifugal high-G simulator," *2017 IEEE International Conference on Systems, Man, and Cybernetics SMC2017*, Banff, Canada (2017).
32. S. Pedrammehr, S. Nahavandi, and H. Abdi, "Closed-form dynamics of hexarot parallel manipulator by means of the principle of virtual work," *Acta Mech. Sin.* 34, 883–895 (2018).
33. S. Pedrammehr, S. Nahavandi, and H. Abdi, "Evaluation of inverse dynamics of hexarot-based centrifugal simulators," *Int. J. Dyn. Control* 6, 1505–1515 (2018).
34. S. Pedrammehr, B. Danaei, H. Abdi, M. T. Masuleh, and S. Nahavandi, "Dynamic analysis of Hexarot: axis symmetric parallel manipulator," *Robotica* 36, 225–240 (2018).
35. S. Pedrammehr, "Dynamic modelling of hexarot parallel mechanisms for design and development," PhD Thesis, Deakin University, Australia (2018).
36. D. Stewart, "A platform with six degrees of freedom," *Proc. Inst. Mech. Eng.* 180, 371–386 (1965).
37. M. J. Tajari, S. Pedrammehr, M. R. C. Qazani, and M. J. Nategh, "The effects of joint clearance on the kinematic error of the hexapod tables," *2017 5th RSI International Conference on Robotics and Mechatronics ICRoM*, Tehran, Iran (2017) pp. 39–44.
38. M. R. C. Qazani, S. Pedrammehr, and M. J. Nategh, "An investigation on the motion error of machine tools' hexapod table," *Int. J. Precis. Eng. Man.* 19, 463–471 (2018).
39. S. Pedrammehr, S. Nahavandi, and H. Asadi, "The forced vibration analysis of hexarot parallel mechanisms," *The 20th IEEE International Conference on Industrial Technology IEEE-ICIT 2019*, Melbourne, Australia (2019).
40. S. Pedrammehr, M. R. C. Qazani, and S. Nahavandi, "A novel axis symmetric parallel mechanism with coaxial actuated arms," *The 4th International Conference on Control, Automation and Robotics, ICCAR 2018*, Auckland, New Zealand (2018).
41. S. Pedrammehr, M. R. C. Qazani, H. Asadi, and S. Nahavandi, "Kinematic manipulability analysis of hexarot simulators," *The 20th IEEE International Conference on Industrial Technology IEEE-ICIT 2019*, Melbourne, Australia (2019).
42. S. Pedrammehr, M. R. C. Qazani, H. Asadi, and S. Nahavandi, "Control system development of a hexarot-based high-G centrifugal simulator," *The 20th IEEE International Conference on Industrial Technology IEEE-ICIT 2019*, Melbourne, Australia (2019).
43. S. Pedrammehr, M. R. C. Qazani, H. Asadi, and S. Nahavandi, "Mathematical modelling of linear motion error for Hexarot parallel manipulators," *Appl. Math. Model* 40, 942–954 (2016)
44. M. Isaksson, T. Brogårdh, and S. Nahavandi, "Parallel manipulators with a rotation-symmetric arm system," *J. Mech. Des.* 134, 114503 (2012).
45. J. P. Merlet, *Parallel Robots*, vol. 128 (Springer Science & Business Media, Dordrecht, 2006).
46. H. D. Taghirad, *Parallel Robots: Mechanics and Control* (CRC press, Boca Raton, 2013).
47. A. Mohammadi, H. Asadi, S. Mohamed, K. Nelson, and S. Nahavandi, "Future reference prediction in model predictive control based driving simulators," *Australasian Conference on Robotics and Automation*, (ACRA, Brisbane, Australia, 2016).

https://doi.org/10.1017/S0263574719000602 Published online by Cambridge University Press

48. H. Asadi, C. Lim, A. Mohammadi, S. Mohamed, S. Nahavandi, and L. Shanmugam, "A genetic algorithm-based nonlinear scaling method for optimal motion cueing algorithm in driving simulator. Proceedings of the Institution of Mechanical Engineers," *Part I: J. Syst. Control Eng.* C1, 232, 1025–1038 (2018).
49. A. Mohammadi, H. Asadi, S. Mohamed, K. Nelson, and S. Nahavandi, "MPC-based motion cueing algorithm with short prediction horizon using exponential weighting," *2016 IEEE International Conference on Systems, Man, and Cybernetics*, (SMC, Budapes, Hungary, 2016).
50. H. Asadi, A. Mohammadi, S. Mohamed, C. Lim, A. Khatami, A. Khosravi, and S. Nahavandi, "A Particle Swarm Optimization-based washout filter for improving simulator motion fidelity," *2016 IEEE International Conference on Systems, Man, and Cybernetics*, (SMC, Budapes, Hungary, 2016).
51. H. Asadi, S. Mohamed, K. Nelson, S. Nahavandi, and M. Oladazimi, "An optimal washout filter based on genetic algorithm compensators for improving simulator driver perception," *DSC 2015: Proceedings of the Driving Simulation Conference & Exhibition*, (Max Planck Institute for the Advancement of Science, Munich, Germany, 2015).
52. K. S. Fu, R. C. Gonzalez, and C. S. G. Lee, *Robotics Control, Sensing, Vision and Intelligence*, 1st ed. (McGraw-Hill Book Company, New York, 1988).
53. S. Pedrammehr,M.Mahboubkhah, and N. Khani, "A study on vibration of Stewart platform-based machine tool table," *Int. J. Adv. Manuf. Technol*. 65, 991–1007 (2013).

Appendix

The physical specifications of the test hexarot manipulators are shown here. All the quantities are in SI units.

Case 1: The general hexarot manipulator

$$a_i = 0.63;\ l_i = 1;\ s_1 = 0.46;\ s_2 = 0.06;$$

$$h_1 = 1.835;\ h_2 = 1.715;\ h_3 = 1.335;\ h_4 = 1.215;\ \ h_5 = 0.835;\ h_6 = 0.715.$$

The mass parameters of the end effector and upper and lower links are:

$$m_p = 5.76;\ m_{p+payload} = 57.6;\ m_a = 7.628;\ m_l = 2.43.$$

The mass center position of the end effector in frame $\{\mathbf{P}\}$:

$${}^{\mathrm{P}}\bar{\mathbf{r}} = \begin{bmatrix} 0 & 0 & 0 \end{bmatrix}^{\mathrm{T}};\ {}^{\mathrm{P}}\bar{\mathbf{r}}_{payload} = \begin{bmatrix} 0 & 0 & 0.1 \end{bmatrix}^{\mathrm{T}}.$$

The length between the mass center of each upper link and the related actuated joint:

$$r_{ai} = 0.248.$$

The length between the mass center of each lower link and the related universal joint:

$$r_{li} = 0.493.$$

The inertia tensor of the end effector in frame $\{\mathbf{P}\}$ is:

$${}^{\mathrm{P}}\mathbf{I}_p = \begin{bmatrix} 0.0404 & 0 & 0 \\ 0 & 0.0404 & 0 \\ 0 & 0 & 0.0808 \end{bmatrix};\ {}^{\mathrm{P}}\mathbf{I}_{p+payload} = \begin{bmatrix} 0.509 & 0 & 0 \\ 0 & 0.509 & 0 \\ 0 & 0 & 0.497 \end{bmatrix}.$$

The inertia tensor of the i^{th} upper link at its mass center is:

$${}^{ai}\mathbf{I}_{ai} = \begin{bmatrix} 1.68 \times 10^{-2} & 0 & 0 \\ 0 & 0.37 & 0 \\ 0 & 0 & 0.37 \end{bmatrix}.$$

The inertia tensor of the i^{th} lower link at its mass center is:

$${}^{li}\mathbf{I}_{li} = \begin{bmatrix} 1.88 \times 10^{-4} & 0 & 0 \\ 0 & 0.198 & 0 \\ 0 & 0 & 0.198 \end{bmatrix}.$$

https://doi.org/10.1017/S0263574719000602 Published online by Cambridge University Press

Coefficients of viscous friction are:

$$C_{Ai} = 0.95;\ C_{Si} = 0.01;\ C_{Ui} = 0.01.$$

Stiffness of the actuators is:

$$K_i = 2.35 \times 10^4.$$

Case 2: The hexarot simulator that is designed for minimum condition number of $\mathbf{J}_p$

$$a_i = 0.63;\ l_i = 0.728;\ \ s_1 = 0.774;\ s_2 = 0.06;$$

$$h_1 = 1.39;\ \ h_2 = 1.287;\ h_3 = 0.848;\ h_4 = 0.742;\ h_5 = 0.303;\ h_6 = 0.197.$$

The mass parameters of the end effector and upper and lower links are:

$$m_p = 17;\ m_{p+payload} = 170;\ m_a = 7.432;\ m_l = 6.192.$$

The mass center position of the end effector in frame $\{\mathbf{P}\}$ is:

$${}^{\mathrm{P}}\bar{\mathbf{r}} = \begin{bmatrix} 0 & 0 & 0 \end{bmatrix}^{\mathrm{T}};\ {}^{\mathrm{P}}\bar{\mathbf{r}}_{payload} = \begin{bmatrix} 0 & 0 & 0.15 \end{bmatrix}^{\mathrm{T}}.$$

The length between the mass center of each upper link and the related actuated joint is:

$$r_{ai} = 0.245.$$

The length between the mass center of each lower link and the related universal joint is:

$$r_{li} = 0.360.$$

The inertia tensor of the end effector in frame $\{\mathbf{P}\}$ is:

$${}^{\mathrm{P}}\mathbf{I}_p = \begin{bmatrix} 0.35 & 0 & 0 \\ 0 & 0.35 & 0 \\ 0 & 0 & 0.70 \end{bmatrix};\ {}^{\mathrm{P}}\mathbf{I}_{p+payload} = \begin{bmatrix} 3.28 & 0 & 0 \\ 0 & 3.28 & 0 \\ 0 & 0 & 3.20 \end{bmatrix}.$$

The inertia tensor of the i^{th} upper link at its mass center is:

$${}^{ai}\mathbf{I}_{ai} = \begin{bmatrix} 2 \times 10^{-2} & 0 & 0 \\ 0 & 0.37 & 0 \\ 0 & 0 & 0.37 \end{bmatrix}.$$

The inertia tensor of the i^{th} lower link at its mass center is:

$${}^{li}\mathbf{I}_{li} = \begin{bmatrix} 4 \times 10^{-3} & 0 & 0 \\ 0 & 0.495 & 0 \\ 0 & 0 & 0.495 \end{bmatrix}.$$

Coefficients of viscous friction are:

$$C_{Ai} = 0.95;\ C_{Si} = 0.01;\ C_{Ui} = 0.01.$$

Stiffness of the actuators is:

$$K_i = 3.4 \times 10^4.$$

https://doi.org/10.1017/S0263574719000602 Published online by Cambridge University Press